Biogeosciences Discuss., 12, 5641–5695, 2015
www.biogeosciences-discuss.net/12/5641/2015/
doi:10.5194/bgd-12-5641-2015

Biogeosciences
Discussions
Open Access

Dynamics of air–sea CO_2 fluxes in the North-West European Shelf based on Voluntary Observing Ship (VOS) and satellite observations

P. Marrec[1,2], T. Cariou[1,2], E. Macé[1,2], P. Morin[1,2], L. A. Salt[1,2], M. Vernet[1,2], B. Taylor[3], K. Paxman[3], and Y. Bozec[1,2]

[1]CNRS, UMR7144, Equipe Chimie Marine, Station Biologique de Roscoff, Place Georges Teissier, 29680 Roscoff, France
[2]Sorbonne Universités, UPMC, Univ. Paris 06, UMR7144, Adaptation et Diversité en Milieu Marin, Station Biologique de Roscoff, 29680 Roscoff, France
[3]Remote Sensing Group, Plymouth Marine Laboratory, Prospect Place PL1 3DH, UK

Received: 25 February 2015 – Accepted: 20 March 2015 – Published: 14 April 2015

Correspondence to: P. Marrec (pmarrec@sb-roscoff.fr)

Published by Copernicus Publications on behalf of the European Geosciences Union.

Abstract

From January 2011 to December 2013, we constructed a comprehensive pCO_2 dataset based on voluntary observing ship (VOS) measurements in the Western English Channel (WEC). We subsequently estimated surface pCO_2 and air–sea CO_2 fluxes in north-west European continental shelf waters using multiple linear regressions (MLRs) from remotely sensed sea surface temperature (SST), chlorophyll *a* concentration (Chl *a*), the gas transfer velocity coefficient (K), photosynthetically active radiation (PAR) and modeled mixed layer depth (MLD). We developed specific MLRs for the seasonally stratified northern WEC (nWEC) and the permanently well-mixed southern WEC (sWEC) and calculated surface pCO_2 with relative uncertainties of 17 and 16 µatm, respectively. We extrapolated the relationships obtained for the WEC based on the 2011–2013 dataset (1) temporally over a decade and (2) spatially in the adjacent Celtic and Irish Seas (CS and IS), two regions which exhibit hydrographical and biogeochemical characteristics similar to those of WEC waters. We validated these extrapolations with pCO_2 data from the SOCAT database and obtained relatively robust results with an average precision of 4 ± 22 µatm in the seasonally stratified nWEC and the southern and northern CS (sCS and nCS), but less promising results in the permanently well-mixed sWEC, IS and Cap Lizard (CL) waters. On an annual scale, seasonally stratified systems acted as a sink of CO_2 from the atmosphere of −0.4, −0.9 and −0.4 $\mathrm{mol\,C\,m^{-2}\,year^{-1}}$ in the nCS, sCS and nWEC, respectively, whereas, permanently well-mixed systems acted as source of CO_2 to the atmosphere of 0.2, 0.4 and 0.4 $\mathrm{mol\,C\,m^{-2}\,year^{-1}}$ in the sWEC, CL and IS, respectively. Air–sea CO_2 fluxes showed important inter-annual variability resulting in significant differences in the intensity and/or direction of annual fluxes. We scaled the mean annual fluxes over six provinces for the last decade and obtained the first annual average uptake of −0.95 $\mathrm{Tg\,C\,year^{-1}}$ for this part of the north-western European continental shelf. Our study showed that combining VOS data with satellite observations can be a powerful tool to estimate and extrapolate air–sea CO_2 fluxes in sparsely sampled area.

1 Introduction

Continental shelf seas, as an interface between land, ocean and atmosphere, host a multitude of biogeochemical processes (Walsh, 1991; Liu et al., 2010) and play a key role in the global carbon cycle (Walsh et al., 1981; Muller-Karger et al., 2005; Bauer et al., 2013). Even though marginal seas occupy only 7 % of global oceanic area, they host enhanced biological activity, which accounts for 15 to 30 % of global oceanic primary production (Gattuso et al., 1998). These productive regions are characterized by enhanced air–sea CO_2 fluxes compared to open oceans (Tsunogai et al., 1999; Thomas et al., 2004) and are particularly vulnerable to anthropogenic forcings such as eutrophication and ocean acidification (Borges and Gypsen, 2010; Borges et al., 2010a; Wallace et al., 2014). In a context of climate change, with rising anthropogenic CO_2 levels in the atmosphere and the oceans (IPCC, 2013), it is essential to better constrain carbon cycle dynamics and particularly air–sea CO_2 fluxes. Given the large diversity and heterogeneity of coastal ecosystems, this goal remains challenging. Rapid expansion of partial pressure of CO_2 ($p$$CO_2$) observations over the past decade have allowed the first assessments of the contribution of coastal ecosystems in terms of global air–sea CO_2 fluxes (Borges et al., 2005; Cai et al., 2006; Chen and Borges, 2009; Cai, 2011). However, extrapolation from local to global estimates still involves large uncertainties and many continental shelf seas remain under-sampled.

Accurate estimates of air–sea CO_2 fluxes in continental shelf seas still suffer from lack of sufficient spatial and temporal coverage. Surveys based on seasonal sampling during oceanographic campaigns and time-series at fixed locations are limited due to the large temporal and spatial variability of these systems. The use of voluntary observing ships (VOS) can improve the coverage of coastal areas at a lesser cost. The recent advances made in this field (Schneider et al., 2006, 2014; Padin et al., 2007; Omar et al., 2010; Marrec et al., 2014) can be combined with other new approaches. Since the 2000 s, $p$$CO_2$ predictions based on remote sensing techniques have been successfully developed for open ocean areas (Lefèvre et al., 2002; Ono et al., 2004;

BGD
12, 5641–5695, 2015

Olsen et al., 2004; Rangama et al., 2005; Gleidhill et al., 2008; Padin et al., 2009; Chierici et al., 2009, 2012). These estimates were based on the use of multiple linear regressions (MLRs) to relate surface ocean pCO_2 to sea surface temperature (SST), chlorophyll *a* concentration (Chl *a*) and occasionally also mixed layer depth (MLD), sea surface salinity (SSS) or geographical position (latitude and longitude). More complex neural networks and self-organizing map techniques have also given promising results (Lefèvre et al., 2005; Telszewski et al., 2009; Friedrich and Oschlies, 2009). In continental shelf seas the development of remotely-sensed approaches is more challenging because of higher temporal and spatial variability of biogeochemical processes. The complex optical properties of these systems can also impede computations based on satellite ocean-color data. These techniques have nevertheless been used to conduct successful assessments of pCO_2 variability in coastal areas (Lohrenz and Cai, 2006; Sallisbury et al., 2008; Borges et al., 2010b; Shadwick et al., 2010; Hales et al., 2012; Jo et al., 2012; Signorini et al., 2013).

To efficiently constrain surface pCO_2 in dynamic shelf seas from remotely sensed data, a comprehensive pCO_2 dataset with sufficient spatial and temporal resolution is essential. In addition to a robust intra-annual temporal resolution, acquisition of pCO_2 measurements over several years is necessary in order to take into consideration the important inter-annual variability of biogeochemical processes in coastal seas. From, 2011 to 2013, we collected an extensive pCO_2 dataset based on VOS observations in the Western English Channel (WEC), which is part of the north-west European continental shelf. We used MLR to develop algorithms to predict surface pCO_2 and air–sea CO_2 fluxes from remotely sensed SST, chlorophyll *a* concentrations (Chl *a*), wind speeds (to calculate the gas transfer velocity coefficient K), photosynthetically active radiation (PAR) and from modeled mixed layer depth (MLD). We extrapolated the relationships obtained in the WEC based on the 2011–2013 dataset (1) temporally over a decade; and (2) spatially in the adjacent Celtic and Irish Seas (CS and IS), two regions where pCO_2 data are very sparse. Based on the reconstructed decadal dataset, we investigated the variability of pCO_2 and air–sea CO_2 fluxes over the shelf.

BGD
12, 5641–5695, 2015

2 Study area

The WEC is part of one of the world's largest margins, the North-West European continental shelf. We studied this area from January 2011 with a VOS (Fig. 1) equipped with an autonomous ocean observing system, called FerryBox, featuring several sensors (Sect. 3.1., Marrec et al., 2013, 2014). This area is characterized by relatively shallow depths and by intense tidal streams with maximum speeds ranging from 0.5 to 2.5 $m s^{-1}$ (Pingree, 1980; Reid et al., 1993). Along the French coast (southern WEC (sWEC)), where the tidal currents are the strongest, the water column remains vertically mixed (Wafar et al., 1983; L'Helguen et al., 1996), whereas near the English coast (northern WEC (nWEC)), where tidal streams are less intense, seasonal stratification occurs (Smyth et al., 2010). Between these two distinct structures, a frontal zone oscillates, separating well-mixed and stratified waters (Pingree et al., 1975). In this complex hydrographical context, high-frequency measurements from FerryBox data allowed us to precisely locate this thermal front and to accurately identify the real extent of each hydrographical province (Marrec et al., 2014).

Satellite SST data (Fig. 2, Sect. 3.2.) combined with Ferrybox measurements allowed us to further define the different hydrographical provinces of the north-west European continental shelf. Water column characteristics similar to those in the WEC are also observed in adjacent seas, i.e. the Irish Sea (IS) and the Celtic Sea (CS) (Pingree and Griffiths, 1978; Pingree, 1980; Holligan, 1981; Simpson, 1981; Hill et al., 2008). Figure 2 shows averaged July and August SST from 2003 to 2013 between 48 and 53° N and 3.5 and 10° W. The coolest surface waters indicate areas where the water column is well-mixed and the warmest SST, areas with seasonal stratification. The Ushant front (Pingree et al., 1975; Morin, 1984; Sournia et al., 1990) separates the seasonally stratified southern Celtic Sea (sCS) and nWEC from the permanently well-mixed sWEC. Such a frontal structure is also observed off the Penwith Peninsula (in the west of Cornwall, UK), around the Cap Lizard (CL) and thereafter we refer to these well-mixed waters as CL. The St. Georges Channel front separates permanently well-mixed south-

BGD
12, 5641–5695, 2015

ern IS (sIS) waters from the seasonally stratified northern CS (nCS) waters. In addition to the similar hydrographical properties, the WEC, CS and IS also exhibited similar seasonal dynamics and biogeochemical processes (Pingree et al., 1978; Pemberton et al., 2004; Smyth et al., 2010). Based on these observations, we defined five key hydrographical provinces (Fig. 2).

We then developed algorithms for both seasonally stratified and permanently well-mixed systems in the WEC (Sect. 3.3.) to estimate surface $p\mathrm{CO_2}$ from environmental variables, and we applied these algorithms in adjacent CS and IS based on satellite and modeled data (Sects. 4.2. and 4.3.). We did not include coastal areas strongly influenced by riverine inputs (Fig. 2) such as the Bristol Channel, coastal Irish waters, surface waters in vicinity of Plymouth and the eastern part of the sIS (which is also seasonally stratified). We chose to study only the southern part of the IS because of the complexity of the northern IS, which has successive stratified, frontal and mixed systems (Simpson and Hunter, 1974) and is influenced by freshwater inputs (Gowen et al., 1995). The study of the permanently well-mixed part of the IS allowed us to apply our algorithm developed for the sWEC to estimate for the first time air–sea $\mathrm{CO_2}$ fluxes in the IS. In the south-west corner of our study area, at the shelf break, internal tides and turbulence favor vertical mixing which sustains biological activity by supplying nutrients to the photic zone (Pingree et al., 1981; Joint et al., 2001; Sharples et al., 2007). Because the internal tides at the shelf break induce specific biogeochemical properties and our algorithms are not intended to predict surface $p\mathrm{CO_2}$ in this province, we excluded the shelf break region (Fig. 1) from our study area.

3 Material and methods

3.1 FerryBox datasets

From January 2011 to January 2014, a FerryBox system was installed on the Voluntary Observing Ship (VOS) Armorique (Brittany Ferries). This vessel crossed the

BGD
12, 5641–5695, 2015

English Channel between Roscoff (France, 48°43′38 N 3°59′03 E) and Plymouth (UK, 50°22′12 N 4°08′31 E) (Fig. 1) up to three times a day. The FerryBox continuously measured sea surface temperature (SST), salinity and partial pressure of CO_2 (pCO_2, from April 2012) along the ferry track with more than 600 crossings with pCO_2 acquisition. Between January 2011 and January 2014, discrete sampling was performed on 57 return crossings between Roscoff and Plymouth with a total of 1026 sampling locations in the WEC. During each cruise, 18 water samples were taken from the FerryBox seawater circuit for the determination of dissolved inorganic carbon (DIC), total alkalinity (TA) and associated salinity and nutrient concentrations (Marrec et al., 2013). Seawater pCO_2 values were calculated from TA, DIC, temperature, salinity and nutrient concentrations with the CO2SYS program (Pierrot et al., 2006) using the equilibrium constants of CO_2 proposed by Mehrbach et al. (1973), refitted by Dickson and Millero (1987) on the seawater pH scale, as recommended by Dickson et al. (2007). The computed values of pCO_2 from DIC and TA have uncertainties of ±5.8 µatm (Zeebe and Wolf-Galdrow, 2001). Sensors were calibrated and/or adjusted based on these bimonthly discrete measurements (Marrec et al., 2014). Based on the comparison between high-frequency pCO_2 data obtained with a Contros HydroC/CO_2 FT sensor and bimonthly pCO_2 data calculated from DIC/TA, we estimated uncertainties relative to high-frequency pCO_2 measurements of ±5.2 µatm (Marrec et al., 2014). We built a composite monthly dataset of in-situ SST and pCO_2 data over 3 years based on both high-frequency and bimonthly measurements. We used bimonthly discrete pCO_2 data between January 2011 and April 2012 and high-frequency pCO_2 data from April 2012 to January 2014. SST monthly means were calculated from FerryBox high-frequency data.

3.2 Satellite and other environmental data

Satellite-derived Chl *a* concentrations (µg L^{-1}) were acquired from the Moderate Resolution Imaging Spectroradiometer (MODIS) aboard the Aqua satellite. Daily images were provided by the Natural Environment Research Council (NERC) Earth Observation Data Acquisition and Analysis Service (NEODAAS) at a spatial resolution of 1.1 km. Monthly mean Chl *a* estimates were computed from January 2003 to December 2013 from these individual images over our study area (Fig. 1). WEC, CS and IS waters are optically complex shelf waters (Joint and Groom, 2000; Darecki et al., 2003; McKee et al., 2007). These shelf seas present both Case 1 and Case 2 optical water types (Morel and Prieur, 1977; Morel et al., 2006) depending on their hydrographical properties (seasonally stratified or homogeneous), the proximity to the coast, and the period of the year. In Case 1 waters, the optical properties are dominated by chlorophyll and associated degradation products as in open ocean waters. In coastal waters, classified as Case 2, suspended particulate sediments and yellow substances of terrestrial origin induce important biases on chlorophyll *a* concentration estimates and special algorithms have been developed for these waters (Gohin et al., 2002). As shown by Groom et al. (2009), who explain how a coastal station in the nWEC (L4) can be considered as Case 1 or Case 2 depending on various parameters, it is difficult to label our studied provinces as Case 1 or Case 2 waters. However sWEC, CL and IS present more similarities with Case 2 waters, especially during winter, whereas nWEC and CS are closer to Case 1 waters. The NEODAAS provided satellite Chl *a* estimates based on the OC3 algorithm, more specific to Case 1 waters, and on the OC5 algorithm (Gohin et al., 2002), developed in the riverine input affected coastal waters of the Eastern English Channel and the Bay of Biscay (Seine, Loire, Gironde). Chl *a* estimates based on the OC3 algorithm show enhanced Chl *a* concentrations during winter, particularly in near-coast and in well-mixed provinces, whereas Chl *a* estimates from the OC5 algorithm tend to underestimate the Chl *a* concentrations especially during spring and summer (data not shown). We chose to use the OC3 algorithm in this study, which seemed more suitable and more representative of the biological activity dynamics, and we binned monthly 1.1 km satellite data into $0.05^{\circ} \times 0.05^{\circ}$ grid cells over our study area. We extracted monthly mean Chl *a* values along the ship track from January 2011 to December 2013 (Fig. 3b) to predict $p\mathrm{CO_2}$ based on MLRs (see below).

Satellite-based SST (°C) data were acquired from the Advanced Very High Resolution Radiometer (AVHRR) instrument. Monthly mean SST estimates were computed from January 2003 to January 2014 from individual images with a spatial resolution of 1.1 km by the NEODAAS. A validation between monthly in-situ SST and associated satellite SST showed a robust correlation ($R^2 = 0.97$, $N = 448$, $p < 0.001$ and RMSE = 0.43). We gridded 1.1 km resolution satellite SST into 0.05° × 0.05° cells as with all other remotely sensed and modeled parameters.

Photosynthetically active radiation (PAR, in $E\,m^{-2}\,d^{-1}$) data were retrieved from the Ocean Biology Processing Group (McClain, 2009; http://oceancolor.gsfc.nasa.gov). We used the Level 3 monthly merged PAR product from MODIS Aqua. PAR were used as a variable in the MLRs as an indicator of the amount of light available for phytoplankton, which presented inter-annual variation over our study period (Fig. 3c). Based on the observations of L'Helguen et al. (1996), Marrec et al. (2014) suggested that light availability might be an important factor responsible for the strong inter-annual variability of phytoplankton blooms in the sWEC.

Mixed layer depth (MLD), which was one of the variables used in algorithm development for the seasonally stratified nWEC and in the spatial extrapolation of this algorithm in the adjacent CS, was computed from the MARS3D model (Lazure and Dumas, 2008; Berger et al., 2014) developed in the PREVIMER project (Charria et al., 2014). MLD was defined as the shallowest depth corresponding to a temperature or density difference with the surface water higher than $\delta T = 0.5\,°C$ or $\delta \mathrm{Dens} = 0.125$ (Monterey and Levitus, 1997). We compared the model outputs with MLD calculated from the temperature and salinity profile at the fixed station E1 off Plymouth (50.03° N, 4.37° W, depth 75 m) from January 2006 to January 2014. Measurements were undertaken fortnightly by the Western Channel Observatory (NERC National Capability of the Plymouth Marine Laboratory and Marine Biological Association, www.westernchannelobservatory.org.uk). Profiles were obtained by a Seabird SBE 19+ with precision for temperature and computed salinity of 0.005 °C and 0.002, respectively. In-situ and modeled MLD at the E1 station showed a good correlation ($R^2 = 0.82$, $N = 89$), validating use of mod-

BGD
12, 5641–5695, 2015

eled MLD in our computations. Modeled MLD were binned in the 0.05° × 0.05° grid in seasonally stratified provinces and were extracted along the ship track in the nWEC to be included in the $p\mathrm{CO_2}$ algorithms. We chose to use the MLD over depth ratio (MLDr) in the MLR computation instead of MLD. During winter in seasonally stratified areas, the whole water column is mixed. However, depths are not homogeneous (ranging from −20 to −200 m), thus the use of MLD winter values, which corresponded approximately to the bathymetry, would lead to bias in MLR computation. MLD, in our algorithms, was only an indicator of the presence or absence of stratification of the water column, particularly concerning the start and the end of stratification. Figure 3e shows the monthly MLDr ratio in the nWEC between Roscoff and Plymouth.

Monthly wind speed data ($\mathrm{m\,s^{-1}}$) corrected to 10 m height were obtained from the NCEP/NCAR re-analysis project (Kalnay et al., 1996) provided by the NOAA-ESRL Physical Sciences Division (Boulder, CO, USA, http://www.esrl.noaa.gov/psd/). We extracted the 2.5° latitude by 2.5° longitude global grid wind speed values over the study area and we binned these data into our 0.05° × 0.05° grid. Wind speed data was used in the computation of the gas transfer velocity of $\mathrm{CO_2}$ (K) used for the calculation of air–sea $\mathrm{CO_2}$ fluxes (Sect. 3.5.) and in algorithm development (Sect. 3.3.) as an indicator of wind stress. Figure 3d shows the monthly computed K values used in the algorithm development along the Ferry route from 2011 to 2013.

3.3 Development of $p\mathrm{CO_2}$ algorithms

We developed two specific algorithms to estimate surface seawater $p\mathrm{CO_2}$ in each of the hydrographical provinces of the WEC (seasonally stratified nWEC and permanently well-mixed sWEC) in order to apply them on a larger spatial and temporal scale in the adjacent Celtic and Irish Seas. We used MLRs to predict $p\mathrm{CO_2}$ in each province based on monthly mean values of Chl *a*, SST, K, the gas transfer velocity (Sect. 3.5.), PAR, MLD (for the nWEC) and from a time variable TI (Eqs. 1 and 2) representative of the seasonality (Friedrich and Oschlies, 2009; Lefèvre et al., 2005; Signorini et al., 2013)

BGD
12, 5641–5695, 2015

according to:

$$pCO_{2,\mathrm{MLR}} = a_0 + \sum_{i=1}^{n} a_i \cdot p_i \tag{1}$$

$$\mathrm{TI} = \sin\left(\frac{2 \cdot \pi \cdot (\mathrm{Day} - \alpha)}{365}\right) \tag{2}$$

where $pCO_{2,\mathrm{MLR}}$ is the predicted pCO_2, a_0 is the intercept of the MLR and a_i is the coefficient related to each variable p_i. In Eq. (2), Day is the 15th day of each month (Julian day) and α a value between 0 and 365 chosen by iteration to optimize the seasonal phasing until the minimum SD on residuals and the best correlation coefficient R^2 are obtained by the MLR. All of these parameters were binned in 0.05° latitude intervals (Figs. 3 and 5) between 48.80° N (off Roscoff) and 50.20° N (off Plymouth). The northern latitude limit of 50.20° N is relatively far from Plymouth in order to exclude effects of freshwater inputs from the Tamar and Plym rivers, which influence the biogeochemical properties of the area (Smyth et al., 2010) and are not representative of nWEC waters. The WEC is divided into sWEC and nWEC at 49.40° N from the average position of the thermal front separating the two hydrographical provinces during the period of study (Fig. 2, and Marrec et al., 2014). MLRs were applied on these binned monthly values in each province using the "*regress*" Matlab® function. The performance of regional algorithms was evaluated by the correlation coefficient R^2, the adjusted R^2, the root-mean-square error (RMSE) and the p values (for each of the parameters and for the regression). The R^2, the adjusted R^2 and RMSE between observed and predicted data represent the capacity (the R^2 and the adjusted-R^2) and uncertainty (RMSE) of the algorithms to predict pCO_2. The coefficient of determination R^2 indicates the amount of total variability explained by the regression mode. The adjusted-R^2 is the coefficient of determination of the MLR adjusted to the degree of freedom, which depends on the number of variables used. In each MLR presented in the study, the adjusted R^2 and R^2 were similar, thus only R^2 is presented.

Discussion Paper | Discussion Paper | Discussion Paper | Discussion Paper |

BGD

12, 5641–5695, 2015

Dynamics of air–sea CO_2 fluxes in the N-W European Shelf

P. Marrec et al.

MLR coefficients were calculated based on our three year dataset and the goal of the study is to apply the algorithms over a decade (2003–2013) over the study area (Fig. 1). The anthropogenic increase in atmospheric CO_2 increases surface ocean $p$$CO_2$ by approximately 1.7 µatm yr^{-1} (Thomas et al., 2008; Le Quéré et al., 2010), equivalent to 17 µatm over 10 years. When we computed the algorithms, we considered this factor in the computations by adding a correction term ΔX (Eq. 3) on the right term of Eq. (1) (Shadwick et al., 2010; Signorini et al., 2013) with

$$\Delta X = \frac{1.7}{12} \cdot \Delta m \tag{3}$$

where Δm (month) is equal to the number of months since July 2012, the middle of our study period (2011–2013). For example, in January 2013, ΔX would be equal to $(1.7/12) \cdot (+6)$ and in January 2012 ΔX would be $(1.7/12) \cdot (-6)$. The same reference month (i.e. July 2012) was used to extrapolate the algorithms from January 2003.

We normalized each of the variables p_i (Eq. 4) using the mean ($p_{i,m}$) and the SD ($p_{i,\text{StdDev}}$) of p_i over study period. The normalized coefficients, which are directly comparable and dimensionless, allowed us to evaluate the relative contribution, or weight, of each of the independent variables (i.e. SST, Chl a, TI, K, PAR and MLD) in the prediction of the dependent variable (i.e. $p\text{CO}_{2,\text{MLR}}$).

$$p_{i,s} = \frac{(p_i - p_{i,m})}{p_{i,\text{StdDev}}} \tag{4}$$

3.4 SOCAT data

The Surface Ocean CO_2 ATlas (SOCAT) database (http://www.socat.info/, Bakker et al., 2014) is an international collection of underway ocean CO_2 measurements. This compilation currently includes approximately 6.3 million measurements from more than 1850 cruises from 1968 to 2011. From January 2003 to January 2011, 46 000 $p$$CO_2$ and associated SST and salinity values were available over the study area (Fig. 4,

BGD
12, 5641–5695, 2015

Table 2). From, 2003 to 2011, in sWEC, nWEC and sCS, pCO_2 values from SOCAT were available for 64 to 79 % of the months (Table 2), mainly from the same south-west/north-east route (Fig. 5) operated principally by three voluntary observing ships (details available on the SOCAT website) which crossed these provinces up to twice per month, almost every month from 2003 to 2011. In nCS and IS, the data coverage was sparser and in CL no data were available. We binned all of these data into the study grid on a monthly basis. The binned data were then averaged over each defined province (Fig. 2, Sect. 2) to compare them to the pCO_2 estimates computed using the algorithms from remotely-sensed data.

3.5 Calculation of air–sea CO_2 fluxes

The fluxes of CO_2 across the air–sea interface (F) were computed from the pCO_2 air–sea gradient ($\Delta pCO_2 = pCO_{2\text{water}} - pCO_{2\text{air}}$, µatm) according to:

$$F = K \cdot \alpha \cdot \Delta pCO_2 \tag{5}$$

where K is the gas transfer velocity ($\mathrm{m\,s^{-1}}$) and α is the solubility coefficient of CO_2 ($\mathrm{mol\,atm^{-1}\,m^{-3}}$) calculated after Weiss (1970). The exchange coefficient K was computed as a function of wind speed with the algorithm given by Nightingale et al. (2000) established in the Southern Bight of the North Sea (SBNS):

$$K = \left(0.222 \cdot u_{10}^2 + 0.333 \cdot u_{10}\right) \cdot \left(\frac{Sc}{660}\right)^{-0.5} \tag{6}$$

where u_{10} is the wind speed data at 10 m height ($\mathrm{m\,s^{-1}}$) and Sc the Schmidt number at in situ SST. The SBNS and the WEC present similar environmental characteristics: these two shallow continental shelves are both close to land with high tidal currents controlling the physical structure of the water column. We also computed gas transfer velocity with the Wanninkhof et al. (1992) and with the Wanninkhof and McGillis (1999) parameterizations for long-term winds to give a range of computed air–sea CO_2

BGD
12, 5641–5695, 2015

fluxes. Wind speeds along the ferry track and over the study area were extracted from monthly wind speed data corrected at 10 m height from the NCEP/NCAR re-analysis project (Sect. 3.2.). Atmospheric pCO_2 (pCO_{2air}) was calculated from the CO_2 molar fraction (xCO_2) at the Mace Head site (53°33′ N 9°00′ W, southern Ireland) of the RAMCES network (Observatory Network for Greenhouse gases) and from the water vapor pressure (pH_2O) using the Weiss and Price (1980) equation. Atmospheric pressure (P_{atm}) over the study area was obtained from the NCEP/NCAR re-analysis project (Kalnay et al., 1996).

4 Results and discussion

4.1 Performance of MLR

We performed MLRs to estimate surface pCO_2 in the nWEC based on SST, Chl *a*, the time variable TI, K and PAR in the sWEC and by including MLDr (MLD/depth ratio). Table 1 shows the MLR normalized coefficients used in the algorithms and their evolutions when we added new variables in the computations. The corresponding R^2 and RMSE are the indicators of the performance of the MLR at each addition of a new variable. Based on SST, Chl *a*, TI, and 398 and 510 monthly gridded observations, we obtained R^2 of 0.65 and 0.79 with RMSE of 21.1 and 18.5 µatm, in the sWEC and nWEC respectively (Table 1). The inclusion of PAR, K and MLDr (only in nWEC) increased R^2 values up to 0.80 and 0.83 in sWEC and nWEC with respective RMSE of 15.8 and 16.9 µatm (Fig. 6a and b). The RMSE accounted for less than 10 % of the amplitude of the pCO_2 signal (approximately 200 µatm). For each variable and each MLR, we calculated the *p* values which were all inferior to 0.001 (not shown in Table 1), meaning that all of the variables were statistically significant in the MLR.

From the normalized coefficients, we calculated the percentages of variability explained by each variable. Normalized coefficients showed that in both provinces, TI contributed to half of the predicted pCO_2 (Table 1). The seasonal pCO_2 signal, which

BGD
12, 5641–5695, 2015

was strongly controlled by biological processes (Marrec et al., 2013), followed an average dynamic closed to a sinusoidal signal. Therefore, the time variable TI contributed to more than half of the variability of the pCO_2 signal, highlighting the strong seasonality observed on this signal (Fig. 5a). Beside TI, the most significant variables in terms of relative contribution were SST and PAR, with 22 and 15 % in sWEC and both with 15 % in nWEC, respectively. Chl *a* contributed for 7 and 6 % in the sWEC and nWEC, respectively, a relatively low value considering that, as reported by Marrec et al. (2013), biological processes are the main driver of seasonal pCO_2 variability in the WEC. The contribution of K in the MLR was small but by adding K in the computation, R^2 increased by 0.02 and 0.01 with a decrease of the RMSE of 0.4 µatm in the sWEC and the nWEC. Similarly, MLDr addition improved the performance of the MLR despite its relatively small contribution compared to the other normalized coefficients. Due to the complexity of the algorithms, a quantitative interpretation of non-normalized coefficients is difficult. For example, according to our model, pCO_2 decreases by 14.3 µatm when SST increases by 1 °C (Table 1). This value is in contradiction with the expected thermodynamic relationship between SST and pCO_2 from Takahashi et al. (1993). The goal of this study was to develop suitable algorithms to predict pCO_2 variability in continental shelf seas by maximizing the performance of the MLR and not to define empirical relationships between the variables and pCO_2.

Figure 5a–c shows the monthly binned (0.05° of latitude) pCO_2, pCO_2 predicted from MLR coefficients ($pCO_{2,MLR}$) and associated residuals ($pCO_{2,obs} - pCO_{2,MLR}$) from January 2011 to January 2014 between Roscoff and Plymouth. As mentioned above, the observed pCO_2 signal was characterized by a strong seasonality with values higher than 450 µatm in autumn and values lower than 300 µatm during spring and summer. As explained by Marrec et al. (2013), in the sWEC the productive period in spring/summer (characterized by pCO_2 decrease due to biological activity) is shorter and less intense than in the nWEC. Furthermore, the sWEC shows enhanced and longer remineralization processes in fall, leading to higher pCO_2 values in homogeneous systems than in stratified systems. Thus, the dynamics of pCO_2 in both provinces presents important inter-annual variability. In the sWEC, pCO_2 values lower than 350 µatm were observed during spring 2011, whereas at the same period of 2012 and 2013, pCO_2 remained close to the atmospheric equilibrium, between 350 and 400 µatm. As the pCO_2 simulation by the MLR is mainly driven by a seasonal cycle (TI), which is the same every year, these inter-annual discrepancies can yield bias in the MLR simulation. For the sWEC the MLR model overestimated pCO_2 during spring and summer 2011 (residuals up to 30 µatm, Fig. 5b and c) and underestimated pCO_2 in spring 2012 (residuals down to −50 µatm, Fig. 5b and c) by simulating an average decrease of pCO_2 both years. On Fig. 6c and d, residuals are plotted vs. observed pCO_2 in the sWEC and nWEC, and on Fig. 6e and f monthly mean residuals over each province are plotted vs. months from January 2011 to December 2013. In the sWEC, when observed pCO_2 ($pCO_{2,Obs}$) values were below 350 µatm, as in spring 2011, $pCO_{2,MLR}$ values were much higher than $pCO_{2,Obs}$ and residuals were highly negative. In the sWEC, residuals as a function of the observed pCO_2 were not homogeneously distributed, with high negative residuals when pCO_2 was below 350 µatm and high positive residuals when pCO_2 was over 450 µatm. In the nWEC, the distribution of residuals was more homogeneous; the less pronounced inter-annual variability was responsible for the better performance of the algorithms (R^2) in this part of the WEC.

Shadwick et al. (2010) and Signorini et al. (2013) undertook similar studies on the Scotian Shelf and the north-east American continental shelf, respectively. They estimated pCO_2 as a function of SST, Chl *a* and K, and from SST, salinity, Chl *a* and a time variable (TI), respectively, using MLR. Based on 14 monthly mean values from a high-frequency dataset at a moored buoy, the algorithm developed by Shadwick et al. (2010) attained a R^2 of 0.81 with an associated standard error of 13 µatm. They extrapolated this algorithm over the entire Scotian Shelf region to investigate pCO_2 and air–sea CO_2 fluxes from remotely-sensed data from 1999 to 2008. Signorini et al. (2013) reported R^2 and associated RMSE ranging from 0.42 to 0.87 and from 22.4 to 36.9 µatm, respectively. They divided the north-east American continental shelf into 5 distinct re-

BGD
12, 5641–5695, 2015

gions according to their physical and biogeochemical attributes. Their study was based on SOCAT surface ocean pCO_2 and the environmental variables used to predict pCO_2 came from remotely-sensed and modeled data. The performances of our MLRs are within the same range as those in these previous studies. We developed our algorithms based on a 3 year dataset obtained during highly contrasting years, which contributed to the robustness of our model to predict a representative seasonal cycle of pCO_2 as seen in the nWEC. However, the WEC is a highly dynamic continental shelf ecosystem characterized by strong inter-annual variations. Very exceptional events, inherent to continental shelf areas, remain difficult to simulate with our method, which explain the lower performances of our MLR for the sWEC.

We compared air–sea CO_2 fluxes (Eq. 5) calculated from observed pCO_2 and from pCO_2 simulation (Fig. 7 and Table 3). Figure 7 shows the air–sea CO_2 flux variation in the sWEC and the nWEC based on $pCO_{2,\mathrm{obs}}$ and $pCO_{2,\mathrm{MLR}}$ from January 2011 to January 2014. Fluxes were computed from the mean monthly pCO_2 of each province and the SD on MLR fluxes corresponds to MLR fluxes computed plus and minus the RMSE obtained in the respective provinces (Table 1). Seasonal air–sea CO_2 flux cycles were well described by the algorithm-defined pCO_2, particularly for the nWEC, with both provinces acting as a sink of atmospheric CO_2 during spring and summer and as source of CO_2 to the atmosphere during autumn and winter. The inter-annual variability of pCO_2 observed in the sWEC during spring and summer was also reflected in the flux computations, the fluxes based on MLR overestimating the CO_2 sink in spring 2012. Table 3 reports the annual flux estimates in both provinces based on in-situ pCO_2 observations and $pCO_{2,\mathrm{MLR}}$. On an annual scale, the seasonally stratified nWEC waters acted as a sink of atmospheric CO_2 at a rate of 0.1 to 0.4 $\mathrm{mol\,C\,m^{-2}\,year^{-1}}$ based on in-situ pCO_2 measurements. Fluxes computed from $pCO_{2,\mathrm{MLR}}$ also indicated that the nWEC acts as a sink of atmospheric CO_2, but we observed some discrepancies between the magnitude of in-situ and MLR based fluxes in 2011 and 2013. The permanently well-mixed sWEC waters acted as a source of CO_2 to the atmosphere from 2011 to 2013 ranging between 0.4 and 0.6 $\mathrm{mol\,C\,m^{-2}\,year^{-1}}$, and annual CO_2 fluxes

BGD
12, 5641–5695, 2015

computed from observed and modeled pCO_2 were in good agreement. The performances of our algorithms to estimate monthly surface pCO_2 allowed us to compute suitable air–sea CO_2 fluxes in WEC provinces during three contrasted years.

4.2 Spatial and temporal extrapolation of the algorithms

We applied the previous algorithms (Sect. 4.1.) over our study area (Fig. 2) from monthly mean remotely-sensed SST, Chl *a*, PAR, and K (based on wind speeds) in the permanently well-mixed sWEC, IS and CL and by adding modeled MLD in the seasonally stratified nWEC, sCS and nCS. The pCO_2 values computed from these variables were averaged by province from January 2003 to December 2013 (Fig. 8). The available SOCAT pCO_2 data (Fig. 4 and Table 2) were binned into $0.05^\circ \times 0.05^\circ$ grid cells and averaged over the provinces. SOCAT pCO_2 monthly mean data were superimposed on the algorithm pCO_2 time series (Fig. 8, red dots).

For the nWEC (Fig. 8d), the comparison between predicted and SOCAT pCO_2 values showed that SOCAT data fitted well with computed pCO_2. The SOCAT data followed the main features of the seasonal cycle described by the model and are in relatively good quantitative agreement. Spring pCO_2 minima were in the same range, despite the discrepancy of time-scales. During autumn and winter, maximum values were not always reached, suggesting a relatively small overestimation of modeled pCO_2 values. In the sCS (Fig. 8c), where SOCAT data covered most months from 2003 to 2011, observed data fitted reasonably well the predicted pCO_2 during spring and summer. During autumn and winter, the model predicted surface water pCO_2 oversaturations compared to atmospheric equilibrium, but only few SOCAT pCO_2 data were above equilibrium values. The limited amount of SOCAT data available for the nCS and IS did not show any major discrepancy with the predicted pCO_2. For the sWEC (Fig. 8e), the predicted pCO_2 values were higher than the data from SOCAT, our algorithm thus mainly overestimating the pCO_2. During spring, the minimal SOCAT pCO_2 values were rarely reached by the model. Figure 4 shows that the SOCAT data available for the sWEC were acquired along the Ushant front (Pingree et al., 1975; Morin, 1984; Sournia

BGD
12, 5641–5695, 2015

et al., 1990) at the border of the province (sWEC, nWEC and sCS) delimited based on summer SST (Fig. 2). This border is a frontal zone between well-mixed and stratified systems with enhanced biological activity due to the constant supply of nutrients from the deep layer of stratified systems, especially in summer when the winter nutrient stock is totally depleted (Holligan, 1981; Morin, 1984; Le Fèvre, 1986; Le Boyer et al., 2009). This enhanced productivity might induce biological consumption of CO_2 which would explain the overestimation of modeled pCO_2 in the frontal zone. The SOCAT data were not representative of a homogeneous system, hindering a direct comparison.

Directly comparing monthly mean pCO_2 values obtained from algorithms and the SOCAT pCO_2 data could generate an important bias because of the timescale difference between these datasets. Monthly gridded SOCAT data were mainly based on measurements performed at daily scales. Computed pCO_2 values were representative of the average monthly pCO_2 variability, which tends to smooth extreme values obtained at shorter timescales and prevent any observation of short-term processes. Despite this time-scale discrepancy the mean differences between predicted and observed pCO_2 were 1 ± 25 µatm in the sCS, 4 ± 24 µatm in the nWEC and 7 ± 17 µatm in the nCS, on an annual scale. Considering the uncertainties relative to the MLR of 17 µatm (Sect. 4.1.), these results are very promising and allowed us to validate the extrapolation of our method over our study area. The results obtained in the sWEC were less promising as explained above and in Sect. 4.1. The comparison with SOCAT data provided indications on the MLR performance on a wider spatial scale. For the first time, we thus computed the seasonal and long-term dynamics of pCO_2 and associated air–sea CO_2 fluxes over a decade for this part of the north-western European continental shelf (Sect. 4.3.) despite the relative uncertainties inherent to the method.

BGD
12, 5641–5695, 2015

4.3 Dynamics of pCO_2 and air–sea CO_2 fluxes

4.3.1 Seasonal variability of pCO_2 and air–sea CO_2 fluxes in stratified systems

Figures 9 to 13 show the monthly values of SST, Chl *a*, computed pCO_2 and associated air–sea CO_2 fluxes in the stratified and homogeneous regions of our study area defined on Fig. 2. Based on in-situ MLD data at fixed station E1 (Western Channel Observatory of Plymouth, Fig. 1) and on modeled MLD (Sect. 3.2., data not shown), we generally observed an onset of stratification in the nWEC and CS from April to October. Modeled MLD data indicated that water column stratification generally started one month earlier and ended one month later in the CS than in the nWEC. The formation of shallow surface layers (≈ 30 m in the CS and 15 m in the nWEC) triggers the initiation of spring phytoplankton blooms in the CS and nWEC (Pingree, 1980). The earlier onset of stratification in the CS than in the nWEC, due to less intense tidal streams (Pingree, 1980), is consistent with the preliminary signs of the spring bloom observed firstly in the CS (Fig. 10). In the CS, the April and May spring bloom, characterized by Chl *a* values between 1 and 5 $\mu g\,L^{-1}$, was followed by low surface Chl *a* concentrations (< 1 $\mu g\,L^{-1}$) for the rest of the year because of total nutrient depletion in the surface layer after the spring bloom. In the nWEC, spring phytoplankton blooms occurred from May and Chl *a* values remained between 1 and 2 $\mu g\,L^{-1}$ until September with particularly elevated Chl *a* in July, as previously reported by Smyth et al. (2010). pCO_2 values below 350 µatm were first observed in the CS from April and one month after in the nWEC (Fig. 11). Surface waters were undersaturated in CO_2 with respect to the atmosphere (Figs. 8 and 11) in seasonally stratified systems from February to October. This pCO_2 undersaturation is mainly driven by thermodynamical processes in February and March and by biological processes until October (Marrec et al., 2013). After the spring phytoplankton blooms, pCO_2 values remained low until September despite the apparent lack of biological activity in surface waters. However, subsurface phytoplankton blooms can occur within the thermocline at the interface with the deep cold water pool, which is not depleted in nutrients (Pemberton

BGD
12, 5641–5695, 2015

et al., 2004; Southward et al., 2005; Smyth et al., 2010). The nWEC and CS waters acted as a sink of atmospheric CO_2 during this period with monthly mean air–sea CO_2 flux values between 0 and $-0.4\,\mathrm{mol\,C\,m^{-2}\,month^{-1}}$ (Figs. 12 and 13). The lowest $p\mathrm{CO_2}$ values were recorded in May in the CS and in July in the nWEC, consistent with previous Chl *a* observations. From September to November, organic matter remineralization processes and the breakdown of stratification increased surface $p\mathrm{CO_2}$ and resulted in $p\mathrm{CO_2}$ oversaturation of surface waters with respect to the atmosphere. During this period, the nWEC and the CS acted as a source of CO_2 to the atmosphere at a rate of 0 to $0.3\,\mathrm{mol\,C\,m^{-2}\,month^{-1}}$.

4.3.2 Seasonal variability of $p\mathrm{CO_2}$ and air–sea CO_2 fluxes in permanently well-mixed systems

The study of the seasonal dynamics of Chl *a* from satellite observations in the all-year well-mixed sWEC, CL and IS is more complex than in adjacent seasonally stratified systems. In the IS, we obtain abnormally high Chl *a* satellite estimates based on the OC3 algorithm (Sect. 3.2.) most of the year caused by elevated suspended particles and colored dissolved organic matter concentrations (McKee and Cunningham, 2006). However, Chl *a* has a minor contribution (7 %, Table 1) in the computation of $p\mathrm{CO_2}$ in homogeneous systems and does not have a large effect on $p\mathrm{CO_2}$ prediction. The areas defined as sWEC and CL are not only representative of homogeneous systems, they also include tidal mixing frontal zones. These frontal regions host higher biological production than well-mixed systems (Pingree et al., 1975). The CL area is almost entirely influenced by these thermal fronts due to its small size, whereas they only impact the sWEC area at its borders (Ushant Front). On monthly mean satellite data, it clearly appeared that enhanced biological activity occurred at the border of the sWEC (Fig. 10). In the central part of the sWEC, Chl *a* values remained low ($< 1\,\mathrm{\mu g\,L^{-1}}$) for most of the year, except in June where a spring phytoplankton bloom was observed. As reported by previous studies (Boalch et al., 1978; L'Helguen et al., 1986; Wafar et al., 1983), the main factor controlling phytoplankton production was light availability. In June, day length is the longest and meteorological conditions are generally favorable, which explains the peak in Chl *a* values. In all-year well-mixed provinces, the lowest pCO_2 values were observed in June (Figs. 8 and 11) with minima around 320 µatm. During autumn, pCO_2 values reached maximum values around 450 µatm caused by organic matter remineralization processes. Biological processes are the main driver of pCO_2 variability in the WEC (Marrec et al., 2013) and this biological control is representative of temperate coastal ecosystems in Europe (Borges et al., 2006; Bozec et al., 2005, 2006). The productive period is shorter in all-year well-mixed systems than in seasonally stratified areas (Marrec et al., 2013, 2014). Surface pCO_2 values were below the atmospheric equilibrium from March to July in the sWEC, CL and IS, whereas these patterns are observed from February to September in the CS and the nWEC (Figs. 8 and 12 and 13).

4.3.3 Variability of air–sea CO_2 fluxes over the shelf and the decade

On an annual scale, the permanently well-mixed sWEC, IS and CL acted as source of CO_2 to the atmosphere at a mean rate (from 2003 to 2013) of 0.2, 0.4 and 0.4 mol C m^{-2} $year^{-1}$, respectively (Table 4), whereas the seasonally stratified systems acted as sinks of atmospheric CO_2, with mean values over 11 years of −0.4, −0.9 and −0.4 mol C m^{-2} $year^{-1}$ for the nCS, sCS and nWEC, respectively (Table 4). Air–sea CO_2 fluxes computed from predicted pCO_2 corroborate the hypothesis of Borges et al. (2005), with permanently well mixed systems acting as sources of CO_2 to the atmosphere and seasonally stratified systems acting as a sink of atmospheric CO_2. The only previous flux estimate for the CS was based on a study by Frankignoulle and Borges (2001), reported in Borges et al. (2006), which indicated that the CS acts as sink of CO_2 of −0.8 mol C m^{-2} $year^{-1}$. In the sCS we obtained an averaged flux value of −0.9 mol C m^{-2} $year^{-1}$, which is in agreement with this previous study. Further, we report what is, to the best of our knowledge, the first estimate of air–sea CO_2 flux in the

IS of 0.4 mol C m^{-2} $year^{-1}$. These values are all in the same order as the mean annual air–sea CO_2 flux value of −1.9 mol C m^{-2} $year^{-1}$ for European coastal waters reported by Borges et al. (2006). The good agreement between the compilations of annually integrated fluxes computed from field measurements by Borges et al. (2006) and the results found in this study confirm the robustness of our MLR.

Our study provides a first assessment of the seasonality of $p\mathrm{CO_2}$ and air–sea CO_2 fluxes over 11 years, but also of the inter-annual and multi-annual variability. Monthly surface ocean $p\mathrm{CO_2}$ derived from algorithms (Fig. 8) showed important inter-annual variability for the seasonal cycle of CO_2 in each province. Monthly air–sea CO_2 fluxes (Fig. 13) followed the same trend as $p\mathrm{CO_2}$, resulting in significant inter-annual differences in the intensity and/or direction of annual fluxes (Table 4 and Fig. 13). The IS and CL remained overall annual sources of CO_2 to the atmosphere from 2003 to 2013, except in 2007 when they acted as sinks of atmospheric CO_2. In the sWEC, the annual 11 year average flux value of 0.2 mol C m^{-2} $year^{-1}$ corresponds to annual values ranging from −0.5 to 0.6 mol C m^{-2} $year^{-1}$. The sWEC acted as a sink of atmospheric CO_2 in 2006 and 2007, and as a source of CO_2 to the atmosphere or neutral for the other years. In, 2007, in permanently well-mixed systems, a particularly intense spring phytoplankton bloom (data not shown) occurred, which resulted in important CO_2 undersaturation and a CO_2 sink. The CO_2 outgassing during autumn 2007 was one of the lowest observed over the decade (Fig. 13), due to relatively weak wind speeds at this time (data not shown) and resulting low K values. The association of these two features explained the annual CO_2 sink obtained in 2007. Seasonally stratified systems showed variability in the intensity of annual air–sea CO_2 fluxes but remained sinks of atmospheric $p\mathrm{CO_2}$ over the decade. In addition to the changes of ocean–atmosphere $p\mathrm{CO_2}$ gradient, the wind-dependent gas transfer velocity has a strong influence on air–sea CO_2 fluxes. For example, during autumn 2009, monthly $p\mathrm{CO_2}$ values were in the same range as the other years (Fig. 8) but we observed peaks of CO_2 outgassing in response to more intense monthly wind speeds (> 10 m s^{-1}). As mentioned above in Sect. 4.1., our method precluded establishment of empirical relationships between the

BGD
12, 5641–5695, 2015

variables and pCO_2, and it is therefore difficult to quantitatively and directly interpret the influence of each variable in the pCO_2 simulation.

We scaled the mean annual fluxes over province areas (Tables 2 and 4) and obtained air–sea CO_2 fluxes of −0.30, −0.72 and −0.05 Tg C year^{-1} in the nCS, sCS and nWEC, and of 0.02, 0.03 and 0.08 Tg C year^{-1} in the sWEC, CL and IS, respectively. These fluxes correspond to absorption of −0.95 Tg C year^{-1} over our study area. Borges et al. (2006) estimated the CO_2 sink over the European continental shelves at −68.1 Tg C year^{-1}, while Chen and Borges (2009) reported air–sea CO_2 flux of −16.1 Tg C year^{-1} in the north-east Atlantic continental shelf region. The contribution of our study area, which represent 5 % of the European continental shelf reported by Borges et al. (2006) appears rather small because of the large extent of well-mixed ecosystems. However, considering the lack of investigation of air–sea CO_2 fluxes in the CS, IS and to a lesser extent in the WEC, our study allowed for the first time to estimate the spatio-temporal dynamics of air–sea CO_2 fluxes in these provinces of the north-west European shelf.

5 Concluding remarks and perspectives

Based on a three-year dataset of pCO_2 measurements acquired on a VOS in the WEC we estimated surface ocean pCO_2 and air–sea CO_2 fluxes in the north-west European continental shelf waters using MLRs from remotely sensed SST, Chl *a*, PAR and wind speed and from modeled MLD (in the nWEC). For the first time, seasonal and long-term dynamics of pCO_2 and over this part of the north-western European continental shelf were evaluated over a decade, despite the relatively high uncertainties inherent to such method. We thus provide the first estimate of air–sea CO_2 flux in the poorly documented CS, IS and WEC. As mentioned above, very few data are currently available in these coastal seas. However, the amount of surface in-situ pCO_2 data grows exponentially and these data are now easily available on data portals as SOCAT to develop and validate such algorithms. For example, in-situ data of the CO_2 system are

BGD
12, 5641–5695, 2015

currently acquired during seasonal cruises within the CANDYFLOSS project (NERC, collaboration National Oceanographic Center/Biological Station of Roscoff) in the CS and the IS, and with a FerryBox system operating between Roscoff (France) and Cork (Ireland). In the future, these data will improve and allow further developments of our algorithms with an adequate division of the shelf area in representative biogeochemical provinces and by developing specific algorithms in each province.

The reconstructed decadal datasets highlighted the importance of multi-annual study of air–sea CO_2 fluxes in continental shelf seas. As mentioned by Keller et al. (2014), it can be difficult to detect relevant trends in the seawater $p\mathrm{CO_2}$ signal, particularly in coastal areas with high inter and intra-annual variability. Beaugrand et al. (2000) and Treguer et al. (2013) demonstrated that coastal marine systems of Western Europe are connected to large scale North-Atlantic atmospheric circulation, the North Atlantic Oscillation (NAO), and there is a consensus that these coastal systems are highly sensitive to natural and anthropogenic climate change (Goberville et al., 2010, 2013). Thomas et al. (2008) investigated the influence of the NAO on air–sea CO_2 fluxes in the North Atlantic and suggested that multi-annual variability of the ocean CO_2 system was linked to the NAO phasing. Salt et al. (2013) demonstrated the connection between NAO forcings and pH and CO_2 variability in the North Sea, another shelf sea of the north-western European continental shelf. We did not attempt an evaluation of the long-term trend of our CO_2 signal as we believe our algorithm needs to be further improved with more in-situ data as mentioned above. In the future, a similar approach could be applied on our dataset to investigate the possible links between large-scale climatic indices and the multi-annual variability of $p\mathrm{CO_2}$ and air–sea CO_2 on this part of the north-western European continental shelf, which is closely connected to North Atlantic open ocean waters.

Acknowledgements. We thank the Brittany Ferries (B.A.I) for providing access to their vessels and especially the captains and crew of the Armorique ferry for their hospitality and their assistance. The authors thank the NERC Earth Observation Data Acquisition and Analysis Service (NEODAAS) for supplying data for this study, especially B. Taylor. We acknowledge the work of the Western Channel Observatory funded under the National Capability of the UK Natural Environmental Research Council for the E1 data. Additional thanks go to G. Charria from IFREMER for providing modelled MLD. We thank M. Ramonet for providing the atmospheric CO_2 data from the RAMCES network (Observatory Network for Greenhouse gases). We thank I. Probert for his help with this manuscript. The Surface Ocean CO_2 Atlas (SOCAT) is an international effort, supported by the International Ocean Carbon Coordination Project (IOCCP), the Surface Ocean Lower Atmosphere Study (SOLAS), and the Integrated Marine Biogeochemistry and Ecosystem Research program (IMBER), to deliver a uniformly quality-controlled surface ocean CO_2 database. The many researchers and funding agencies responsible for the collection of data and quality control are thanked for their contributions to SOCAT. This work was funded by the European Project INTERREG IV/MARINEXUS, by the "Conseil Général du Finistère" (CG29), by the "Region Bretagne" (program ARED, project CHANNEL) and by INSU (program LEFE/CYBER, project CHANNEL). Y. Bozec is P.I. of the CHANNEL project and associate researcher (CR1) at CNRS. P. Marrec holds a Ph.D. grant from the Region Bretagne at the UPMC.

References

Bakker, D. C. E., Pfeil, B., Smith, K., Hankin, S., Olsen, A., Alin, S. R., Cosca, C., Harasawa, S., Kozyr, A., Nojiri, Y., O'Brien, K. M., Schuster, U., Telszewski, M., Tilbrook, B., Wada, C., Akl, J., Barbero, L., Bates, N. R., Boutin, J., Bozec, Y., Cai, W.-J., Castle, R. D., Chavez, F. P., Chen, L., Chierici, M., Currie, K., de Baar, H. J. W., Evans, W., Feely, R. A., Fransson, A., Gao, Z., Hales, B., Hardman-Mountford, N. J., Hoppema, M., Huang, W.-J., Hunt, C. W., Huss, B., Ichikawa, T., Johannessen, T., Jones, E. M., Jones, S. D., Jutterström, S., Kitidis, V., Körtzinger, A., Landschützer, P., Lauvset, S. K., Lefèvre, N., Manke, A. B., Mathis, J. T., Merlivat, L., Metzl, N., Murata, A., Newberger, T., Omar, A. M., Ono, T., Park, G.-H., Paterson, K., Pierrot, D., Ríos, A. F., Sabine, C. L., Saito, S., Salisbury, J., Sarma, V. V. S. S., Schlitzer, R., Sieger, R., Skjelvan, I., Steinhoff, T., Sullivan, K. F., Sun, H., Sutton, A. J., Suzuki, T., Sweeney, C., Takahashi, T., Tjiputra, J., Tsurushima, N., van Heuven, S. M. A. C., Vandemark, D., Vlahos, P., Wallace, D. W. R., Wanninkhof, R., and Watson, A. J.: An update to the Surface Ocean CO_2 Atlas (SOCAT version 2), Earth Sys. Sci. Data, 6, 69–90, doi:10.5194/essd-6-69-2014, 2014.

Bates, N. R., Best, M. H. P., Neely, K., Garley, R., Dickson, A. G., and Johnson, R. J.: Detecting anthropogenic carbon dioxide uptake and ocean acidification in the North Atlantic Ocean, Biogeosciences, 9, 2509–2522, doi:10.5194/bg-9-2509-2012, 2012.

Bauer, J. E., Cai, W.-J., Raymond, P. A., Bianchi, T. S., Hopkinson, C. S., and Regnier, P. A. G.: The changing carbon cycle of the coastal ocean, Nature, 504, 61–70, doi:10.1038/nature12857, 2013.

Beaugrand, G., Ibanez, F., and Reid, P. C.: Spatial, seasonal and long-term fluctuations of plankton in relation to hydroclimatic features in the English Channel, Celtic Sea and Bay of Biscay, Mar. Ecol.-Prog. Ser., 200, 93–102, 2000.

Berger, B. H., Dumas, F., Petton, S., and Lazure, P.: Evaluation of the hydrology and dynamics of the operational Mars3d configuration of the bay of Biscay, Mercator Ocean-Q. Newslett., 49, 60–68, 2014.

Boalch, G. T., Harbour, D. S., and Butler, A. I.: Seasonal phytoplankton production in the western English Channel 1964–1974, J. Mar. Biol. Assoc. UK, 58, 943–953, 1978.

Borges, A. V. and Frankignoulle, M.: Distribution of surface carbon dioxide and air–sea exchange in the English Channel and adjacent areas, J. Geophys. Res., 108, 1–14, doi:10.1029/2000JC000571, 2003.

Borges, A. V. and Gypens, N.: Carbonate chemistry in the coastal zone responds more strongly to eutrophication than to ocean acidification, Limnol. Oceanogr., 55, 1–8, 2010.

Borges, A. V., Delille, B., and Frankignoulle, M.: Budgeting sinks and sources of CO_2 in the coastal ocean: diversity of ecosystems counts, Geophys. Res. Lett., 32, L14601, doi:10.1029/2005GL023053, 2005.

Borges, A. V., Schiettecatte, L.-S., Abril, G., Delille, B., and Gazeau, F.: Carbon dioxide in European coastal waters, Estuar. Coast. Shelf S., 70, 375–387, doi:10.1016/j.ecss.2006.05.046, 2006.

Borges, A. V., Alin, S. R., Chavez, F. P., Vlahos, P., Johnson, K. S., Holt, J. T., Balch, W. M., Bates, N., Brainard, R., Cai, W. J., Chen, C. T. A., Currie, K., Dai, M., Degrandpre, M., Delille, B., Dickson, A., Evans, W., Feely, R. A., Friederich, G. E., Gong, G.-C., Hales, B., Hardman-Mountford, N., Hendee, J., Hernandez-Ayon, J. M., Hood, M., Huertas, E., Hydes, D., Ianson, D., Krasakopoulou, E., Litt, E., Luchetta, A., Mathis, J., McGillis, W. R., Murata, A., Newton, J., Ólafsson, J., Omar, A., Perez, F. F., Sabine, C., Salisbury, J. E., Salm, R., Sarma, V. V. S. S., Schneider, B., Sigler, M., Thomas, H., Turk, D., Vandemark, D., Wanninkhof, R., Ward, B.: A global sea surface carbon observing system: inorganic and organic carbon dynamics in coastal oceans, in: Proceedings of OceanObs'09: Sustained Ocean Observations and Information for Society (Vol. 2), Venice, Italy, 21–25 September 2009, edited by: Hall, J., Harrison, D. E., and Stammer, D., ESA Publication WPP-306, doi:10.5270/OceanObs09.cwp.07, 2010a.

Borges, A. V., Ruddick, K., Lacroix, G., Nechad, B., Asteroca, R., Rousseau, V., and Harlay, J.: Estimating pCO_2 from remote sensing in the Belgian coastal zone, ESA. Special. Publ., 686, 2–7, 2010b.

Bozec, Y., Thomas, H., Elkalay, K., and de Baar, H. J. W.: The continental shelf pump for CO_2 in the North Sea – evidence from summer observation, Mar. Chem., 93, 131–147, doi:10.1016/j.marchem.2004.07.006, 2005.

Bozec, Y., Thomas, H., and Schiettecatte, L.-S.: Assessment of the processes controlling seasonal variations of dissolved inorganic carbon in the North Sea, Limnol. Oceanogr., 51, 2746–2762, 2006.

Cai, W.-J.: Estuarine and coastal ocean carbon paradox: CO_2 sinks or sites of terrestrial carbon incineration?, Annu. Rev. Mar. Sci., 3, 123–145, doi:10.1146/annurev-marine-120709-142723, 2011.

Cai, W.-J., Dai, M., and Wang, Y.: Air–sea exchange of carbon dioxide in ocean margins: a province-based synthesis, Geophys. Res. Lett., 33, 1–4, doi:10.1029/2006GL026219, 2006.

Charria, G. and Repecaud, M.: PREVIMER: a contribution to in situ coastal observing systems, Mercator Ocean-Q. Newslett., 49, 9–20, 2014.

Chen, C. A. and Borges, A. V.: Reconciling opposing views on carbon cycling in the coastal ocean?: continental shelves as sinks and near-shore ecosystems as sources of atmospheric CO_2, Deep-Sea Res. Pt. II, 56, 578–590, doi:10.1016/j.dsr2.2008.12.009, 2009.

Chierici, M., Olsen, A., Johannessen, T., Trinañes, J., and Wanninkhof, R.: Algorithms to estimate the carbon dioxide uptake in the northern North Atlantic using shipboard observations, satellite and ocean analysis data, Deep-Sea Res. Pt. II, 56, 630–639, doi:10.1016/j.dsr2.2008.12.014, 2009.

Chierici, M., Signorini, S. R., Mattsdotter-Björk, M., Fransson, A., and Olsen, A.: Surface water fCO_2 algorithms for the high-latitude Pacific sector of the Southern Ocean, Remote Sens. Environ., 119, 184–196, doi:10.1016/j.rse.2011.12.020, 2012.

BGD
12, 5641–5695, 2015

Dynamics of air–sea CO_2 fluxes in the N-W European Shelf

P. Marrec et al.

Darecki, M., Weeks, A., Sagan, S., Kowalczuk, P., and Kaczmarek, S.: Optical characteristics of two contrasting Case 2 waters and their influence on remote sensing algorithms, Cont. Shelf Res., 23, 237–250, doi:10.1016/S0278-4343(02)00222-4, 2003.

Dickson, A. G. and Millero, F. J.: A comparison of the equilibrium constants for the dissociation of carbonic acid in seawater media, Deep-Sea Res., 34, 1733–1743, 1987.

Dickson, A. G., Sabine, C. L., and Christian, J. R.: Guide to best practices for ocean CO_2 measurements, PICES Special Publication 3, IOCCP report No. 8, North Pacific Marine Science Organization and Sidney, British Columbia, 191 pp., 2007.

Dumousseaud, C., Achterberg, E. P., and Tyrrell, T., Charalampopoulou, A., Schuster, U., Hartman, M., and Hydes, D. J.: Contrasting effects of temperature and winter mixing on the seasonal and inter-annual variability of the carbonate system in the Northeast Atlantic Ocean, Biogeosciences, 7, 1481–1492, doi:10.5194/bg-7-1481-2010, 2010.

Friedrich, T. and Oschlies, A.: Neural network-based estimates of North Atlantic surface $p\mathrm{CO}_2$ from satellite data: a methodological study, J. Geophys. Res., 114, 1–12, doi:10.1029/2007JC004646, 2009.

Gattuso, J. P., Frankignoulle, M., and Wollast, R.: Carbon and carbonate metabolism in coastal aquatic ecosystems, Annu. Rev. Ecol. Sys., 29, 405–434, 1998.

Gledhill, D. K., Wanninkhof, R., Millero, F. J., and Eakin, M.: Ocean acidification of the Greater Caribbean Region 1996–2006, J. Geophys. Res., 113, 1–11, doi:10.1029/2007JC004629, 2008.

Goberville, E., Beaugrand, G., Sautour, B., Tréguer, P., and Somlit, T.: Climate-driven changes in coastal marine systems of western Europe, Mar. Ecol.-Prog. Ser., 408, 129–147, doi:10.3354/meps08564, 2010.

Goberville, E., Beaugrand, G., and Edwards, M.: Synchronous response of marine plankton ecosystems to climate in the Northeast Atlantic and the North Sea, J. Marine Syst., 129, 189–202, doi:10.1016/j.jmarsys.2013.05.008, 2014.

Gohin, F., Druon, J. N., and Lampert, L.: A five channel chlorophyll concentration algorithm applied to SeaWiFS data processed by SeaDAS in coastal waters, Int. J. Remote. Sens., 23, 1639–1661, 2002.

Gowen, R. J. and Stewart, B. M.: Regional differences in stratification and its effect on phytoplankton production and biomass in the northwestern Irish Sea, J. Plankton Res., 17, 753–769, 1995.

BGD
12, 5641–5695, 2015

Groom, S., Martinez-Vicente, V., Fishwick, J., Tilstone, G., Moore, G., Smyth, T., and Harbour, D.: The Western English Channel observatory: optical characteristics of station L4, J. Marine Syst., 77, 278–295, doi:10.1016/j.jmarsys.2007.12.015, 2009.

Hales, B., Strutton, P. G., Saraceno, M., Letelier, R., Takahashi, T., Feely, R., Sabine, C., and Chavez, F.: Satellite-based prediction of $p\mathrm{CO_2}$ in coastal waters of the eastern North Pacific, Prog. Oceanogr., 103, 1–15, doi:10.1016/j.pocean.2012.03.001, 2012.

Hickman, A., Moore, C., Sharples, J., Lucas, M., Tilstone, G., Krivtsov, V., and Holligan, P.: Primary production and nitrate uptake within the seasonal thermocline of a stratified shelf sea, Mar. Ecol.-Prog. Ser., 463, 39–57, doi:10.3354/meps09836, 2012.

Hill, E., Brown, J., Fernand, L., Holt, J., Horsburgh, K. J., Proctor, R., Raine, R., and Turrell, W. R.: Thermohaline circulation of shallow tidal seas, Geophys. Res. Lett., 35, L11605, doi:10.1029/2008GL033459, 2008.

Holligan, P. M.: Biological implications of fronts on the northwest European continental shelf, Philos. T. R. Soc. S-A, 302, 547–562, 1981.

IPCC: Climate Change 2013: The physical science basis, in: Contribution of Working Group I to the Fifth Assessment Report of the Intergovernmental Panel on Climate Change, edited by: Stocker, T. F., Qin, D., Plattner, G.-K., Tignor, M., Allen, S. K., Boschung, J., Nauels, A., Xia, Y., Bex, V., and Midgley, P. M., Cambridge University Press, Cambridge, UK and New York, NY, USA, 1535 pp., 2013.

Jo, Y.-H., Dai, M., Zhai, W., Yan, X.-H., and Shang, S.: On the variations of sea surface $p\mathrm{CO_2}$ in the northern South China Sea: a remote sensing based neural network approach, J. Geophys. Res., 117, 1–13, doi:10.1029/2011JC007745, 2012.

Joint, I. and Groom, S.: Estimation of phytoplankton production from space: current status and future potential of satellite remote sensing, J. Exp. Mar. Biol. Ecol., 250, 233–255, 2000.

Joint, I., Wollast, R., Chou, L., Batten, S., Elskens, M., Edwards, E., Hirst, A., Burkill, P., Groom, S., Gibb, S., Miller, A., Hydes, D., Dehairs, F., Antia, A., Barlow, R., Rees, A., Pomroy, A., Brockmann, U., Cummings, D., Lampitt, R., Loijens, M., Mantoura, F., Miller, P., Raabe, T., Alvarez-Salgado, X., Stelfox, C., and Woolfenden, J.: Pelagic production at the Celtic Sea shelf break, Deep-Sea Res. Pt. II, 48, 3049–3081, doi:10.1016/S0967-0645(01)00032-7, 2001.

Kalnay, E., Kanamitsu, M., Kistler, R., Collins, W., Deaven, D., Gandin, L., Iredell, M., Saha, S., White, G., Woollen, J., Zhu, Y., Chelliah, M., Ebisuzaki, W., Higgins, W., Janowlak, J.,

Discussion Paper | Discussion Paper | Discussion Paper | Discussion Paper |

Mo, K. C., Ropelewski, C., Wang, J., Leetmaa, A., Reynolds, R., Jenne, R., and Joseph, D.: The NCEP/NCAR reanalysis project, B. Am. Meteorol. Soc., 77, 437–471, 1996.
Keller, K. M., Joos, F., and Raible, C. C.: Time of emergence of trends in ocean biogeochemistry, Biogeosciences, 11, 3647–3659, doi:10.5194/bg-11-3647-2014, 2014.
Kitidis, V., Hardman-Mountford, N. J., Litt, E., Brown, I., Cummings, D., Hartman, S., Hydes, D., Fishwick, J. R., Harris, C., Martinez-Vicente, V., Woodward, E. M. S., and Smyth, T. J.: Seasonal dynamics of the carbonate system in the Western English Channel, Cont. Shelf Res., 42, 30–40, doi:10.1016/j.csr.2012.04.012, 2012.
L'Helguen, S., Madec, C., and Le Corre, P.: Nitrogen uptake in permanently well-mixed temperate coastal waters, Estuar. Coast. Shelf S., 42, 803–818, doi:10.1006/ecss.1996.0051, 1996.
Lazure, P. and Dumas, F.: An external–internal mode coupling for a 3-D hydrodynamical model for applications at regional scale (MARS), Adv. Water Resour., 31, 233–250, doi:10.1016/j.advwatres.2007.06.010, 2008.
Le Boyer, A., Cambon, G., Daniault, N., Herbette, S., Le Cann, B., Marié, L., and Morin, P.: Observations of the Ushant tidal front in September 2007, Cont. Shelf Res., 29, 1026–1037, doi:10.1016/j.csr.2008.12.020, 2009.
Le Fèvre, J.: Aspects of the biology of frontal systems, Adv. Mar. Biol., 23, 163–299, 1986.
Le Quéré, C., Takahashi, T., Buitenhuis, E. T., Rödenbeck, C., and Sutherland, S. C.: Impact of climate change and variability on the global oceanic sink of CO_2, Global Biogeochem. Cy., 24, GB4007, doi:10.1029/2009GB003599, 2010.
Lefèvre, N., Aiken, J., Rutllant, J., Daneri, G., Lavender, S., and Smyth, T.: Observations of pCO$_2$ in the coastal upwelling off Chile: spatial and temporal extrapolation using satellite data, J. Geophys. Res., 107, 3055, doi:10.1029/2000JC000395, 2002.
Lefèvre, N., Watson, A. J., and Watson, A. R.: A comparison of multiple regression and neural network techniques for mapping in situ pCO$_2$ data, Tellus B, 57, 375–384, 2005.
Liu, K.-K., Atkinson, L., Quinones, R., and Talaue-McManus, L. (eds.): Carbon and Nutrient Fluxes in Continental Margins A Global Synthesis, IGBP Book Series, Springer, Heidelberg, Germany, 744 pp., 2010.
Lohrenz, S. E. and Cai, W.-J.: Satellite ocean color assessment of air–sea fluxes of CO_2 in a river-dominated coastal margin, Geophys. Res. Lett., 33, 2–5, doi:10.1029/2005GL023942, 2006.

BGD
12, 5641–5695, 2015

Marrec, P., Cariou, T., Collin, E., Durand, A., Latimier, M., Macé, E., Morin, P., Raimund, S., Vernet, M., and Bozec, Y.: Seasonal and latitudinal variability of the CO_2 system in the western English Channel based on Voluntary Observing Ship (VOS) measurements, Mar. Chem., 155, 29–41, 2013.
Marrec, P., Cariou, T., Latimier, M., Macé, E., Morin, P., Vernet, M., and Bozec, Y.: Spatiotemporal dynamics of biogeochemical processes and air–sea CO_2 fluxes in the Western English Channel based on two years of FerryBox deployment, J. Marine Syst., 140, 26–38, doi:10.1016/j.jmarsys.2014.05.010, 2014.
McClain, C. R.: A decade of satellite ocean color observations, Annu. Rev. Mar. Sci., 1, 19–42, doi:10.1146/annurev.marine.010908.163650, 2009.
McKee, D. and Cunningham, A.: Identification and characterisation of two optical water types in the Irish Sea from in situ inherent optical properties and seawater constituents, Estuar. Coast. Shelf S., 68, 305–316, doi:10.1016/j.ecss.2006.02.010, 2006.
McKee, D., Cunningham, A., and Dudek, A.: Optical water type discrimination and tuning remote sensing band-ratio algorithms: application to retrieval of chlorophyll and Kd(490) in the Irish and Celtic Seas, Estuar. Coast. Shelf S., 73, 827–834, doi:10.1016/j.ecss.2007.03.028, 2007.
Mehrbach, C., Culberso, C., Hawley, J. E., and Pytkowic, R. M.: Measurement of apparent dissociation constants of carbonic acid in seawater at atmospheric pressure, Limnol. Oceanogr., 18, 897–907, 1973.
Monterey, G. and Levitus, S.: Seasonal variability of mixed layer depth for the world ocean, NOAA Atlas, NESDIS 14, Washington DC, 96 pp, 1997.
Morel, A. and Prieur, L.: Analysis of variations in ocean color, Limnol. Oceanogr., 22, 709–722, doi:10.4319/lo.1977.22.4.0709, 1977.
Morel, A., Gentili, B., Chami, M., AND Ras, J.: Bio-optical properties of high chlorophyll Case 1 waters and of yellow-substance-dominated Case 2 waters, Deep-Sea Res. Pt. I, 53, 1439–1459, doi:10.1016/j.dsr.2006.07.007, 2006.
Morin, P.: Evolution des éléments nutritifs dans les systems frontaux de l'Iroise: assimilation et regeneration; relation avec les structures hydrologiques et les cycles de développemnt du phytoplankton, Ph.D. thesis in the Univ. Bretagne Occid., 320 pp., Brest, France, 1984.
Muller-Karger, F. E., Varela, R., Thunell, R., Luerssen, R., Hu, C., and Walsh, J. J.: The importance of continental margins in the global carbon cycle, Geophys. Res. Lett., 32, L01602, doi:10.1029/2004GL021346, 2005.

BGD
12, 5641–5695, 2015

Nightingale, P. D., Malin, G., Law, C. S., Watson, A. J., Liss, P. S., Liddicoat, M. I., Boutin, J., and Upstill-Goddard, R. C.: In situ evaluation of air–sea gas exchange parameterizations using novel conservative and volatile tracers, Global Biogeochem. Cy., 14, 373–387, 2000.

Olsen, A., Triñanes, J., and Wanninkhof, R.: Sea–air flux of CO_2 in the Caribbean Sea estimated using in situ and remote sensing data, Remote Sens. Environ., 89, 309–325, doi:10.1016/j.rse.2003.10.011, 2004.

Omar, A. M., Olsen, A., Johannessen, T., Hoppema, M., Thomas, H., and Borges, A. V.: Spatiotemporal variations of $f\mathrm{CO_2}$ in the North Sea, Ocean Sci., 6, 77–89, doi:10.5194/os-6-77-2010, 2010.

Ono, T., Saino, T., Kurita, N., Sasaki, K.: Basin-scale extrapolation of shipboard $p\mathrm{CO_2}$ data by using satellite SST and Chl *a*, Int. J. Remote. Sens., 25, 3803–3815, 2004.

Padin, X. A., Vazquezrodriquez, M., Rios, A. F., and Perez, F. F.: Surface CO_2 measurements in the English Channel and Southern Bight of North Sea using voluntary observing ships, J. Marine Syst., 66, 297–308, doi:10.1016/j.jmarsys.2006.05.011, 2007.

Padin, X. A., Navarro, G., Gilcoto, M., Rios, A. F., and Pérez, F. F.: Estimation of air–sea CO_2 fluxes in the Bay of Biscay based on empirical relationships and remotely sensed observations, J. Marine Syst., 75, 280–289, doi:10.1016/j.jmarsys.2008.10.008, 2009.

Pemberton, K., Rees, A. P., Miller, P. I., Raine, R., and Joint, I.: The influence of water body characteristics on phytoplankton diversity and production in the Celtic Sea, Cont. Shelf. Res., 24, 2011–2028, doi:10.1016/j.csr.2004.07.003, 2004.

Pierrot, D., Lewis, E., and Wallace, D. W. R.: MS Excel Program Developed for CO_2 System Calculations, ORNL/CDIAC-105, Carbon Dioxide Information Analysis Center, Oak Ridge National Laboratory, US Department of Energy, Oak Ridge, Tennessee, 2006.

Pingree, R. D., Pugh, P. R., Holligan, P. M., and Forster, G. R.: Summer phytoplankton blooms and red tides along tidal fronts in the approaches to the English Channel, Nature, 258, 672–677, 1975.

Pingree, R. D.: Physical oceanography of the Celtic Sea and the English Channel, in: The Northwest European Shelf Seas: The Sea-Bed and the Sea in Motion, edited by: Banner, F. T., Collins, B., and Massie, K. S., Elsevier, Amsterdam, 638 pp., 1980.

Pingree, R. D. and Griffiths, D. K.: Tidal fronts on the shelf seas around the British Isles, J. Geophys. Res., 83, 4615–4622, 1978.

Pingree, R. D., Holligan, P. M., Mardell, G. T.: The effects of vertical stability on phytoplankton distributions in the summer on the northwest European Shelf, Deep-Sea Res., 25, 1011–1028, 1978.
Pingree, R. D., Mardell, G. T., and Cartwright, D. E.: Slope turbulence, internal waves and phytoplankton growth at the Celtic Seas shelf-break, Philos. T. R. Soc. S-A, 302, 663–682, 1981.
Rangama, Y., Boutin, J., Etcheto, J., Merlivat, L., Takahashi, T., Delille, B., Frankignoulle, M., and Bakker, D. C. E.: Variability of the net air–sea CO_2 flux inferred from shipboard and satellite measurements in the Southern Ocean south of Tasmania and New Zealand, J. Geophys. Res., 110, 1–17, doi:10.1029/2004JC002619, 2005.
Reid, P. C., Auger, C., Chaussepied, M., and Burn, M.: The channel, report on sub-region 9, quality status report of the North Sea 1993, UK Dep. of the Environ., Républ. Fr. Minist. de l'Environ., Inst. Fr. de Rech. Pour l'Exploit. de la Mer, Brest. 153 pp., 1993.
Salisbury, J., Vandemark, D., Hunt, C., Campbell, J., McGillis, W., and Mcdowell, W.: Seasonal observations of surface waters in two Gulf of Maine estuary-plume systems: relationships between watershed attributes, optical measurements and surface $p\mathrm{CO_2}$, Estuar. Coast. Shelf S., 77, 245–252, doi:10.1016/j.ecss.2007.09.033, 2008.
Salt, L. A., Thomas, H., Prowe, A. E. F., Borges, A. V., Bozec, Y., de Baar, H. J. W.: Variability of North Sea pH and CO_2 in response to North Atlantic Oscillation forcing, J. Geophys. Res., 118, 1584–1592, doi:10.1002/2013JG002306, 2013.
Schneider, B., Kaitala, S., and Maunula, P.: Identification and quantification of plankton bloom events in the Baltic Sea by continuous $p\mathrm{CO_2}$ and chlorophyll *a* measurements on a cargo ship, J. Marine Syst., 59, 238–248, doi:10.1016/j.jmarsys.2005.11.003, 2006.
Schneider, B., Gustafsson, E., Sadkowiak, B.: Control of the mid-summer net community production and nitrogen fixation in the central Baltic Sea: an approach based on $p\mathrm{CO_2}$ measurements on a cargo ship, J. Marine Syst., 136, 1–9, doi:10.1016/j.jmarsys.2014.03.007, 2014.
Shadwick, E. H., Thomas, H., Comeau, A., Craig, S. E., Hunt, C. W., and Salisbury, J. E.: Air–Sea CO_2 fluxes on the Scotian Shelf: seasonal to multi-annual variability, Biogeosciences, 7, 3851–3867, doi:10.5194/bg-7-3851-2010, 2010.
Sharples, J. and Tweddle, J. F.: Spring-neap modulation of internal tide mixing and vertical nitrate fluxes at a shelf edge in summer, Limnol. Oceanogr., 52, 1735–1747, 2007.

Signorini, S. R., Mannino, A., Najjar, R. G., Friedrichs, M. A. M., Cai, W.-J., Salisbury, J., Wang, Z. A., Thomas, H., and Shadwick, E. H.: Surface ocean pCO_2 seasonality and sea–air CO_2 flux estimates for the North American east coast, J. Geophys. Res., 118, 5439–5460, doi:10.1002/jgrc.20369, 2013.
Simpson, J. H. and Hunter, J. R.: Fronts in the Irish Sea, Nature, 250, 404–406, 1974.
Simpson, J. H., Crisp, D. J., and Hearn, C.: The shelf-sea fronts: implications of their existence and behavior, Philos. T. R. Soc. S-A., 302, 531–546, 1981.
Smyth, T. J., Fishwick, J. R., AL-Moosawi, L., Cummings, D. G., Harris, C., Kitidis, V., Rees, A., Martinez-Vicente, V., and Woodward, E. M. S.: A broad spatio-temporal view of the Western English Channel observatory, J. Plankton Res., 32, 585–601, doi:10.1093/plankt/fbp128, 2009.
Sournia, A., Brylinski, J. M., and Dallot, S.: Fronts hydrologiques au large des côtes françaises: les sites-ateliers de programme Frontal, Oceanol. Acta., 13, 413–438, 1990.
Southward, A. J., Langmead, O., Hardman-Mountford, N. J., Aiken, J., Boalch, G. T., Dando, P. R., Genner, M. J., Joint, I., Kendall, M. A., Halliday, N. C., Harris, R. P., Leaper, R., Mieszkowska, N., Pingree, R. D., Richardson, A. J., Sims, D. W., Smith, T., Walne, A. W., and Hawkins, S. J.: Long-term oceanographic and ecological research in the Western English Channel, Adv. Mar. Biol., 47, 1–105, 2005.
Telszewski, M., Chazottes, A., Schuster, U., Watson, A. J., Moulin, C., Bakker, D. C. E., González-Dávila, M., Johannessen, T., Körtzinger, A., Lüger, H., Olsen, A., Omar, A., Padin, X. A., Ríos, A. F., Steinhoff, T., Santana-Casiano, M., Wallace, D. W. R., and Wanninkhof, R.: Estimating the monthly pCO_2 distribution in the North Atlantic using a self-organizing neural network, Biogeosciences, 6, 1405–1421, doi:10.5194/bg-6-1405-2009, 2009.
Thomas, H., Bozec, Y., Elkalay, K., and de Baar, H. J. W.: Enhanced open ocean storage of CO_2 from shelf sea pumping, Science, 304, 1005–1008, doi:10.1126/science.1095491, 2004.
Thomas, H., Bozec, Y., Elkalay, K., de Baar, H. J. W., Borges, A. V., and Schiettecatte, L.-S.: Controls of the surface water partial pressure of CO_2 in the North Sea, Biogeosciences, 2, 323–334, doi:10.5194/bg-2-323-2005, 2005.
Thomas, H., Prowe, F., van Heuven, S., Bozec, Y., de Baar, H. J. W., Schiettecatte, L.-S., Suykens, K., Kone', M., Borges, A. V., Lima, I. D., and Doney, S. C.: Rapid decline of the CO_2 buffering capacity in the North Sea and implications for the North Atlantic Ocean, Global Biogeochem. Cy., 21, GB4001, doi:10.29/2006GB002825, 2007.

BGD
12, 5641–5695, 2015

Dynamics of air–sea CO_2 fluxes in the N-W European Shelf

P. Marrec et al.

Thomas, H., Prowe, F. E., Lima, I. D., Doney, S. C., Wanninkhof, R., Greatbatch, R. J., Schuster, U., and Corbière, A.: Changes in the North Atlantic Oscillation influence CO_2 uptake in the North Atlantic over the past 2 decades, Global Biogeochem. Cy., 22, GB4027, doi:10.1029/2007GB003167, 2008.

Tréguer, P., Goberville, E., Barrier, N., L'Helguen, S., Morin, P., Bozec, Y., Rimmelin-Maury, P., Czamanski, M., Grossteffan, E., Cariou, T., Répécaud, M., Quéméner, L.: Large and local-scale influences on physical and chemical characteristics of coastal waters of Western Europe during winter, J. Marine Syst., 139, 79–90, doi:10.1016/j.jmarsys.2014.05.019, 2014.

Tsunogai, S., Watanabe, S., Sato, T.: Is there a "continental shelf pump" for the absorption of atmospheric CO_2?, Tellus B., 51, 701–712, 1999.

Wafar, M. V. M., Corre, P. L., Birrien, J. L.: Nutrients and primary production in permanently well-mixed temperate coastal waters, Estuar. Coast. Shelf S., 17, 431–446, 1983.

Wallace, R. B., Baumann, H., Grear, J. S., Aller, R. C., Gobler, C. J.: Coastal ocean acidification: the other eutrophication problem, Estuar. Coast. Shelf S., 148, 1–13, doi:10.1016/j.ecss.2014.05.027, 2014.

Walsh, J. J.: Importance of continental margins in the marine biogeochemical cycling of carbon and nitrogen, Nature, 350, 53–55, 1991.

Walsh, J. J., Rowe, G. T., Iverson, R. L., McRoy, C. P.: Biological export of shelf carbon is a sink of the global CO_2 cycle, Nature, 291, 196–201, 1981.

Wanninkhof, R.: Relationship between wind speed and gas exchange over the ocean, J. Geophys. Res., 97, 7373–7382, doi:10.1029/92JC00188, 1992.

Wanninkhof, R. and Mcgillis, W. R.: A cubic relationship between air–sea CO_2 exchange and wind speed, Geophys. Res. Lett., 26, 1889–1892, 1999.

Weiss, R. F.: Solubility of nitrogen, oxygen and argon in water and seawater, Deep-Sea Res. 17, 721–735, 1970.

Weiss, R. F. and Price, B. A.: Nitrous oxide solubility in water and seawater, Mar. Chem., 8, 347–359, 1980.

Zeebe, R. E. and Wolf-Gladrow, D. A.: CO_2 in seawater: equilibrium, kinetics, isotopes, Elsevier Oceanography Series, 65, Elsevier, Amsterdam, 346 pp., 2001.

BGD
12, 5641–5695, 2015

Dynamics of air–sea CO_2 fluxes in the N-W European Shelf

P. Marrec et al.

Table 1. MLR normalized coefficients for each variable in sWEC (A, 48.80–49.40 °N) and nWEC (B, 49.40–50.20 °N) with corresponding R^2 and RMSE values. Percentages of variability explained by each variable were computed only when all the variables were included in the MLR. Non-normalized coefficient values are given for the last step of the MLR with their standard error (Std.Err.). N values are the number of values used in the MLR and α is the value between 0 and 365 chosen by iteration to optimize the seasonal phasing.

(A)

Variables	MLR Coeff	1	2	3	% of variability	Coeff. Values	Std.Err.
	a0	397.23	397.88	397.89	–	648.20	17.69
SST	a1	−43.2	−26.2	−28.2	**22.2 %**	−14.2	1.25
CHLA	a2	−15.2	−7.2	−8.2	**6.5 %**	−22.2	2.62
TI	a3	−83.2	−63.2	−67.2	**52.2 %**	−67.2	3.48
PAR	a5	–	−16.2	−19.2	**15.0 %**	−1.2	0.08
K	a6	–	–	−5.2	**4.2 %**	-5.14×10^5	1.11×10^5
	$\boldsymbol{R^2}$	**0.65**	**0.79**	**0.80**		$\boldsymbol{N = 398}$	
	RMSE (µatm)	**21.1**	**16.3**	**15.8**		$\boldsymbol{\alpha = 336}$	$\boldsymbol{p < 0.001}$

(B)

Variables	MLR Coeff	1	2	3	4	% of variability	Coeff. Values	Std.Err.
	a0	377.42	377.43	377.48	377.38	–	450.47	14.03
SST	a1	−12.2	−26.2	−27.2	−19.2	**15.2 %**	−7.2	1.00
CHLA	a2	−7.2	−9.2	−9.2	−8.2	**6.4 %**	−12.2	1.39
TI	a3	−47.2	−74.2	−77.2	−69.2	**53.9 %**	−69.2	4.21
PAR	a5	–	21.66	20.48	19.87	**15.3 %**	1.26	0.19
K	a6	–	–	−3.2	−3.2	**2.7 %**	-3.37×10^5	0.96×10^5
MLD	a7	–	–		−8.2	**6.5 %**	−27.2	4.58
	$\boldsymbol{R^2}$	**0.79**	**0.81**	**0.82**	**0.83**		$\boldsymbol{N = 510}$	
	RMSE (µatm)	**18.5**	**17.7**	**17.3**	**16.9**		$\boldsymbol{\alpha = 26}$	$\boldsymbol{p < 0.001}$

BGD
12, 5641–5695, 2015
Dynamics of air–sea CO_2 fluxes in the N-W European Shelf
P. Marrec et al.

Table 2. Area (in km^2) of each defined province (Fig. 2), number of available SOCAT pCO_2 data and the percentage of available monthly SOCAT pCO_2 data between 2003 and 2011.

Region	Area (km^2)	Nb of Obs.	% Time Coverage
IS	18 115	635	5 %
nCS	58 035	3979	7 %
sCS	65 943	31 079	79 %
nWEC	11 912	9855	77 %
sWEC	12 167	3147	64 %
CL	5412	0	0 %

BGD
12, 5641–5695, 2015

Dynamics of air–sea CO_2 fluxes in the N-W European Shelf

P. Marrec et al.

Table 3. Air–sea CO_2 fluxes (in $mol\,C\,m^{-2}\,year^{-1}$) calculated from observed pCO_2 and from pCO_2 obtained by MLR along the ferry track in nWEC and sWEC using Nightingale et al. (2000) k parametrization. Values in brackets were computed using Wanninkhof et al. (1992) and Wanninkhof and McGillis (1999) k parameterizations for long-term winds to give a range of computed air–sea CO_2 fluxes.

Year	Northern WEC Obs.	MLR	Southern WEC Obs.	MLR
2011	−0.2 (−0.2/ − 0.2)	−0.2 (−0.2/0.2)	0.4 (0.9/0.9)	0.6 (1.2/1.2)
2012	−0.2 (−0.2/ − 0.2)	−0.2 (−0.2/ − 0.2)	0.6 (1.2/1.0)	0.5 (0.9/0.9)
2013	−0.2 (−0.2/0.1)	−0.2 (−0.2/ − 0.2)	0.5 (0.9/0.9)	0.5 (0.9/0.9)

BGD
12, 5641–5695, 2015

Table 4. Annual air–sea CO_2 fluxes (in mol C m^{-2} year^{-1}) in the seasonally stratified (nCS, sCS and nWEC) and permanently provinces (sWEC, CL and IS) of our study area between 2003 and 2013 and the mean annual fluxes over the decade using Nightingale et al. (2000) *k* parametrization. Scaled annual fluxes over province areas (Table 2) in Tg C year^{-1} were calculated from the mean annual fluxes over the decade. Fluxes in brackets were calculated using Wanninkhof et al. (1992) and Wanninkhof and McGillis (1999) *k* parameterizations for long-term winds.

Year	Seasonnaly Stratified nCS	sCS	nWEC	Permanently Mixed sWEC	CL	IS
2003	−0.4 (−0.9/ − 0.4)	−0.9 (−1.9/ − 1.1)	−0.4 (−0.8/ − 0.2)	0.0 (0.0/0.3)	0.3 (0.6/0.7)	0.2 (0.4/0.4)
2004	−0.4 (−0.7/ − 0.3)	−0.8 (−1.6/ − 1.1)	−0.2 (−0.4/0.0)	0.3 (0.4/0.6)	0.6 (1.4/1.2)	0.4 (0.9/0.7)
2005	−0.4 (−0.8/ − 0.2)	−0.9 (−1.9/ − 1.1)	−0.3 (−0.6/ − 0.1)	0.1 (0.0/0.1)	0.4 (0.9/0.9)	0.4 (0.8/0.7)
2006	−0.6 (−1.2/ − 0.6)	−1.2 (−2.4/ − 1.7)	−0.7 (−1.4/ − 0.8)	−0.1 (−0.2/0.0)	0.2 (0.4/0.5)	0.2 (0.3/0.3)
2007	−0.7 (−1.4/ − 0.8)	−1.2 (−2.6/ − 1.9)	−0.9 (−1.9/ − 1.3)	−0.5 (−1.2/ − 0.9)	−0.3 (−0.8/ − 0.5)	0.0 (−0.2/0.0)
2008	−0.4 (−0.7/ − 0.3)	−0.8 (−1.8/ − 1.2)	−0.3 (−0.6/ − 0.2)	0.1 (0.1/0.3)	0.5 (1.0/0.9)	0.5 (0.9/0.7)
2009	−0.3 (−0.5/0.0)	−0.7 (−1.3/ − 0.4)	0.0 (0.1/0.6)	0.6 (1.4/1.8)	0.7 (1.6/1.8)	0.6 (1.3/0.9)
2010	−0.3 (−0.5/ − 0.2)	−0.8 (−1.5/ − 0.9)	−0.1 (−0.1/0.1)	0.5 (1.2/1.0)	0.6 (1.3/1.1)	0.5 (1.2/0.7)
2011	−0.4 (−0.9/ − 0.5)	−0.8 (−1.7/ − 1.1)	−0.3 (−0.7/ − 0.3)	0.3 (0.6/0.5)	0.4 (0.9/0.8)	0.3 (0.7/0.5)
2012	−0.4 (−0.9/ − 0.5)	−0.8 (−1.6/ − 1.1)	−0.2 (−0.5/ − 0.2)	0.3 (0.6/0.5)	0.7 (1.4/1.1)	0.5 (0.9/0.6)
2013	−0.6 (−1.3/ − 0.7)	−1.2 (−2.7/ − 1.9)	−0.5 (−1.1/ − 0.6)	0.0 (−0.1/0.0)	0.4 (0.8/0.7)	0.3 (0.6/0.5)
Mean (mol C m^{-2} yr^{-1})	−0.4 (−0.9/ − 0.4)	−0.9 (−1.9/ − 1.2)	−0.4 (−0.7/ − 0.3)	0.2 (0.3/0.4)	0.4 (0.9/0.8)	0.4 (0.7/0.5)
Mean (Tg C yr^{-1})	−0.30 (−0.62/ − 0.28)	−0.72 (−1.52/ − 0.97)	−0.05 (−0.10/ − 0.04)	0.02 (0.04/0.05)	0.03 (0.06/0.05)	0.08 (0.15/0.12)

BGD
12, 5641–5695, 2015

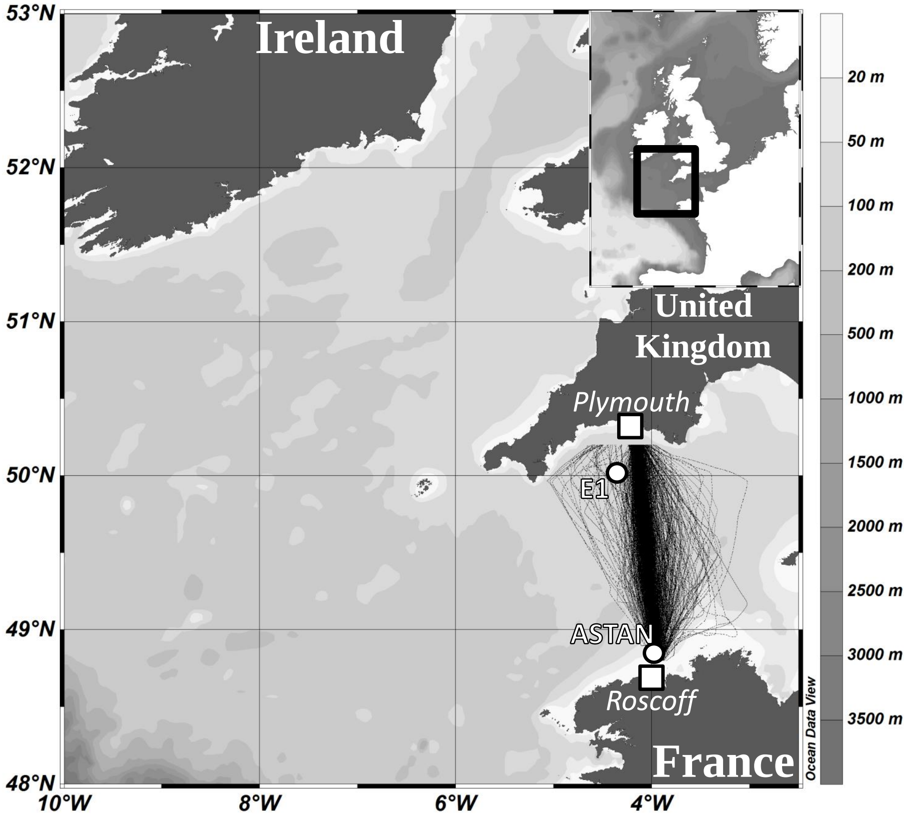

Figure 1. Map and bathymetry of the study area with the tracks of all crossings made from 2011 to 2013 by the ferry *Armorique* between Roscoff (France) and Plymouth (UK). The location of fixed stations E1 (Western Channel Observatory) and ASTAN (coastal observatory SOMLIT) are also indicated.

BGD
12, 5641–5695, 2015

Dynamics of air–sea CO_2 fluxes in the N-W European Shelf

P. Marrec et al.

Title Page
Abstract | Introduction
Conclusions | References
Tables | Figures
◂◂ | ▸▸
◂ | ▸
Back | Close
Full Screen / Esc
Printer-friendly Version
Interactive Discussion

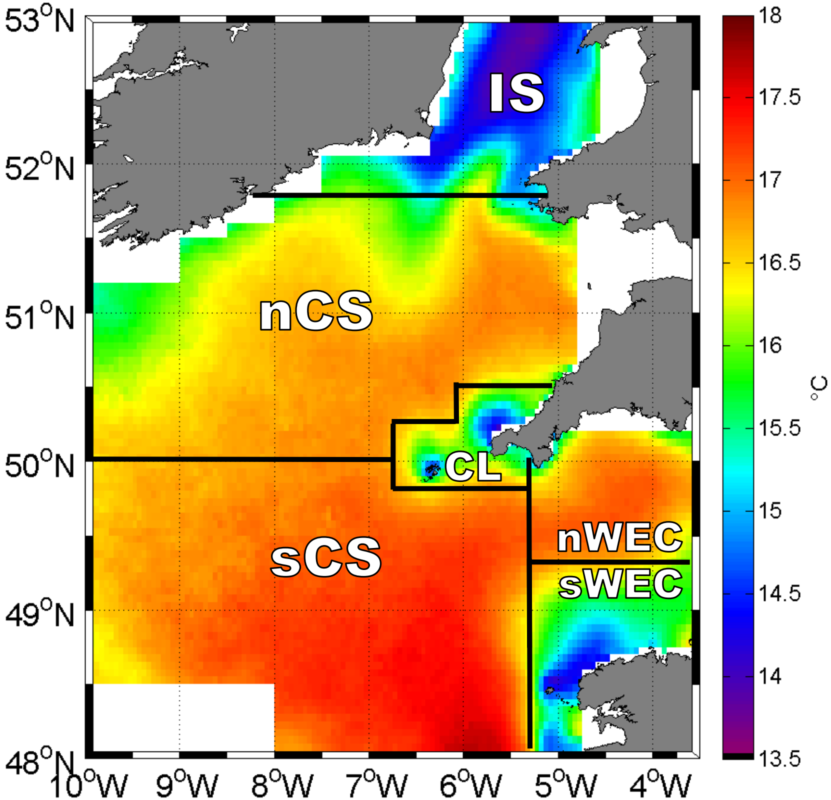

Figure 2. Mean July and August satellite SST (°C) between 2003 and 2013 with delimitation of defined hydrographical provinces: Irish Sea (IS), northern Celtic Sea (nCS), southern CS (sCS), Cap Lizard province (CL), northern Western English Channel (nWEC) and southern WEC (sWEC). The warmest SST are characteristic of seasonally stratified areas and the coldest of permanently well-mixed systems.

BGD
12, 5641–5695, 2015

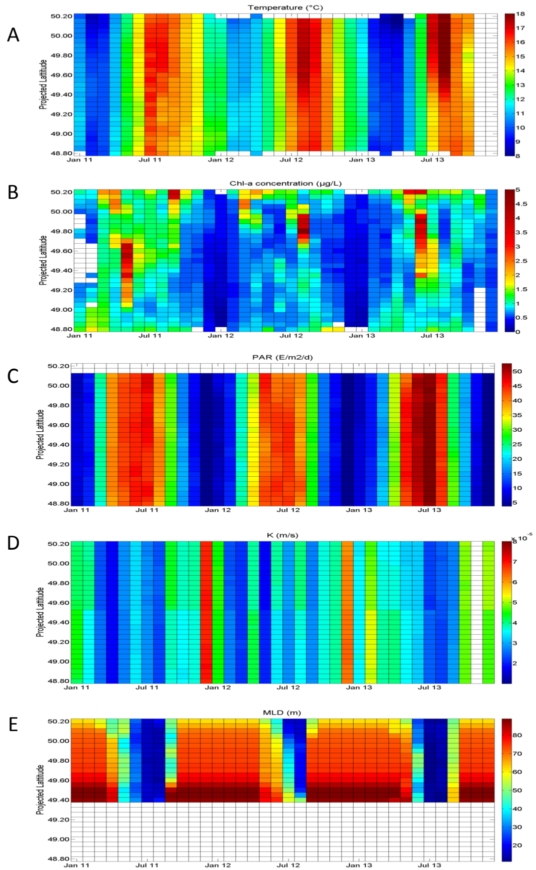

Figure 3. Distribution of monthly gridded **(a)** SST (°C), **(b)** Chl *a* ($\mu g\,L^{-1}$), **(c)** PAR ($E\,m^{-2}\,d^{-1}$), **(d)** K ($m\,s^{-1}$) and **(e)** MLD over depth ratio MLDr in the WEC between Roscoff and Plymouth from January 2011 to December 2013.

BGD
12, 5641–5695, 2015

Dynamics of air–sea CO_2 fluxes in the N-W European Shelf

P. Marrec et al.

Title Page
Abstract | Introduction
Conclusions | References
Tables | Figures
◀| |▶
◀ ▶
Back | Close
Full Screen / Esc
Printer-friendly Version
Interactive Discussion

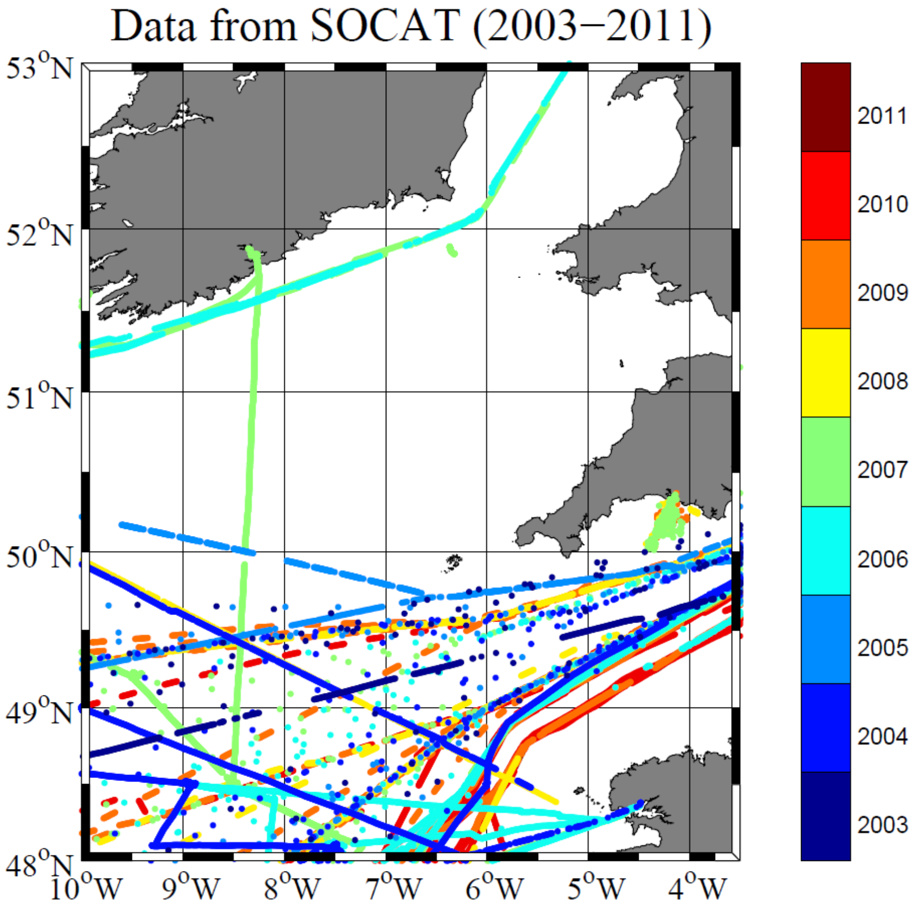

Figure 4. Map of available SOCAT surface pCO_2 data with color-coded respective year of acquisition between 2003 and 2011.

BGD
12, 5641–5695, 2015

Dynamics of air–sea CO_2 fluxes in the N-W European Shelf

P. Marrec et al.

Discussion Paper | Discussion Paper | Discussion Paper | Discussion Paper |

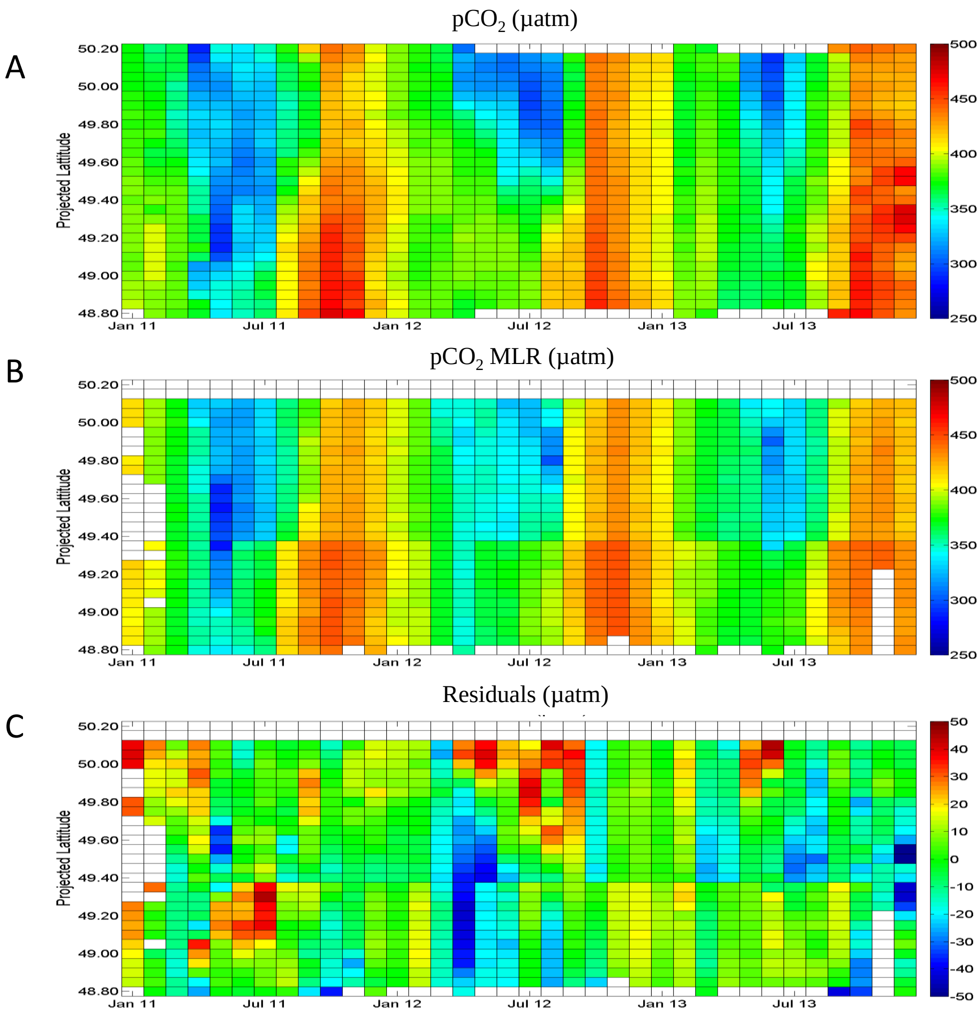

BGD
12, 5641–5695, 2015

Title Page
Abstract | Introduction
Conclusions | References
Tables | Figures
◀| |▶
◀ ▶
Back | Close
Full Screen / Esc
Printer-friendly Version
Interactive Discussion

Figure 5. Distribution of monthly gridded **(a)** pCO_2 (µatm) based on bimonthly DIC/TA measurements (January 2011 to March 2012) and on high-frequency pCO_2 measurements (April 2012 to December 2013) in WEC, **(b)** $pCO_{2,MLR}$ (µatm) computed from nWEC and sWEC algorithms and **(c)** residuals ($pCO_2 - pCO_{2,MLR}$ in µatm) between Roscoff and Plymouth from January 2011 to December 2013.

BGD

12, 5641–5695, 2015

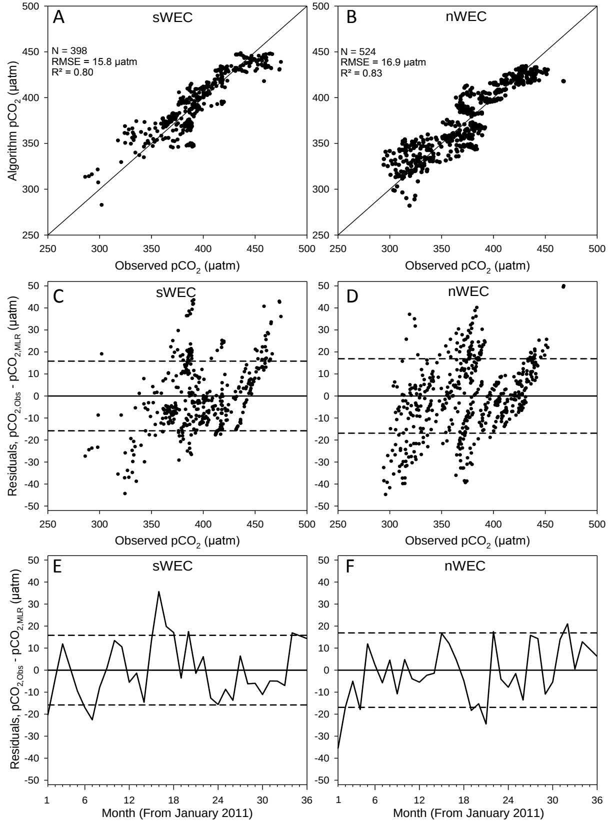

Figure 6. Observed monthly gridded pCO_2 (µatm) vs. $pCO_{2,MLR}$ computed from the algorithms developed in sWEC **(a)** and in nWEC **(b)** with respective number of values (N), R^2 and RMSE. Residuals between observed pCO_2 and predicted pCO_2 in function of observed pCO_2 values (µatm) in sWEC **(c)** and nWEC **(d)**. Mean monthly residuals (µatm) over sWEC **(e)** and nWEC **(f)** in function of the months from January 2011. On plots **(c–f)** the dashed lines represents the RMSE of MLR developed in sWEC (±15.8 µatm) and nWEC (±16.9 µatm).

BGD
12, 5641–5695, 2015

Dynamics of air–sea CO_2 fluxes in the N-W European Shelf

P. Marrec et al.

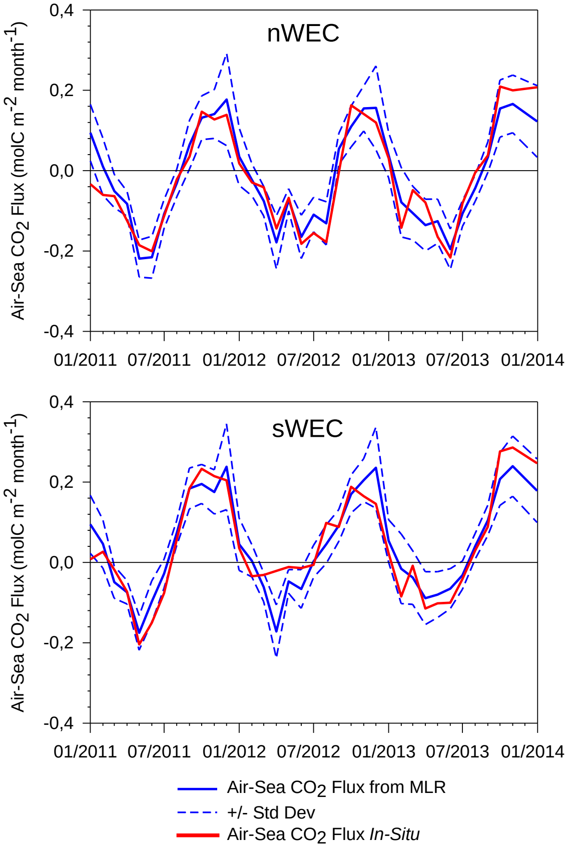

Figure 7. Monthly air–sea CO_2 fluxes (mol C m^{-2} month^{-1}) computed from observed pCO_2 (in red) and $pCO_{2,MLR}$ (in blue) data in nWEC and sWEC from 2011 to 2013 using Nightingale et al. (2000) gas transfer velocity K. Dashed lines represent fluxes computed from $pCO_{2,MLR}$ plus and minus respective RMSE.

BGD
12, 5641–5695, 2015

Dynamics of air–sea CO_2 fluxes in the N-W European Shelf

P. Marrec et al.

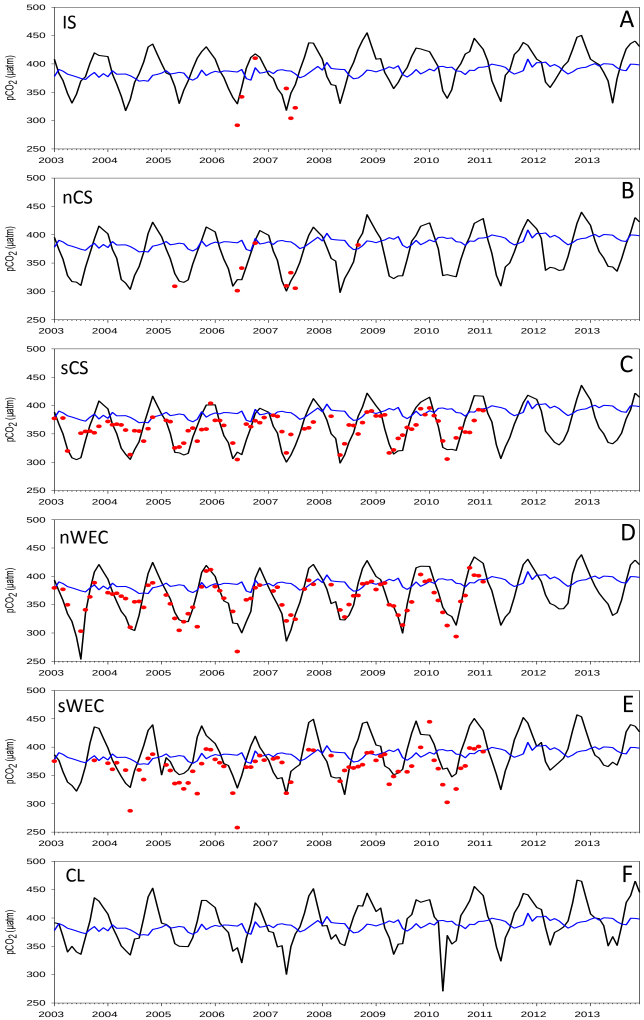

BGD
12, 5641–5695, 2015

Dynamics of air–sea CO_2 fluxes in the N-W European Shelf

P. Marrec et al.

Figure 8. Time series of monthly $pCO_{2,MLR}$ (µatm, in black) averaged over IS **(a)**, nCS **(b)**, sCS **(c)**, nWEC **(d)**, sWEC **(e)** and CL **(f)** provinces from 2003 to 2013. Monthly mean corresponding SOCAT data (red dots) are shown for comparison. The blue lines represent the atmospheric pCO_2.

BGD
12, 5641–5695, 2015

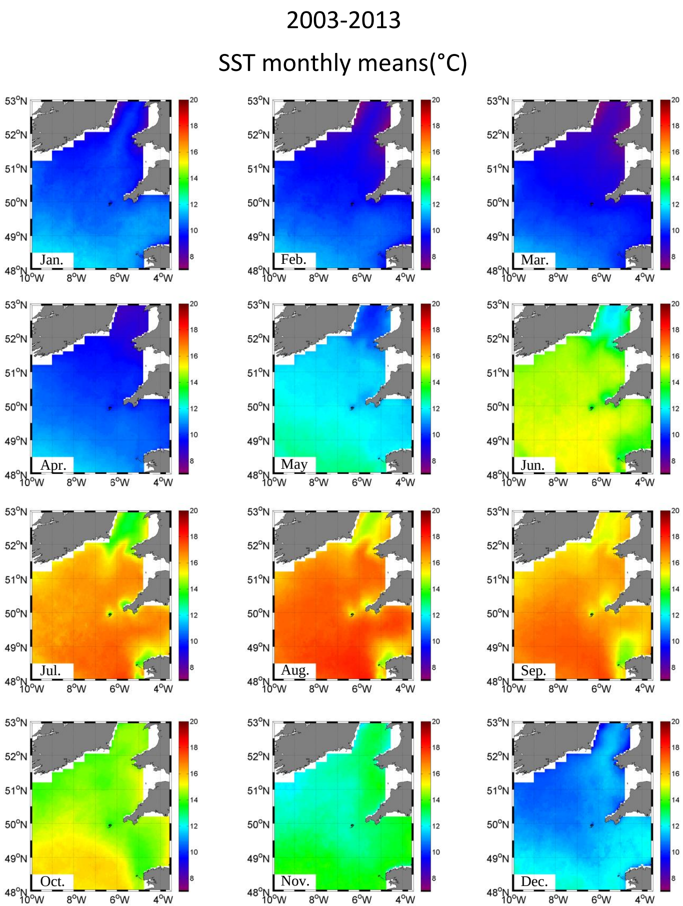

Figure 9. Monthly satellite SST (°C) averaged from 2003 to 2013 from January (top left corner) to December (bottom right corner).

BGD
12, 5641–5695, 2015

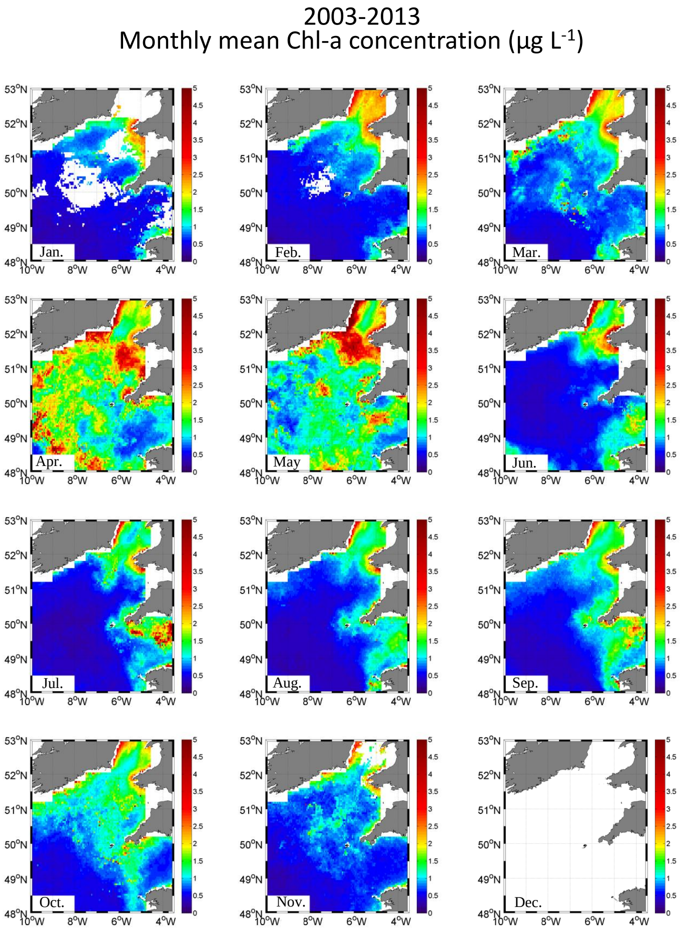

Figure 10. Monthly satellite Chl *a* ($\mu g\,L^{-1}$) averaged from 2003 to 2013 from January (top left corner) to December (bottom right corner).

BGD

12, 5641–5695, 2015

Dynamics of air–sea CO_2 fluxes in the N-W European Shelf

P. Marrec et al.

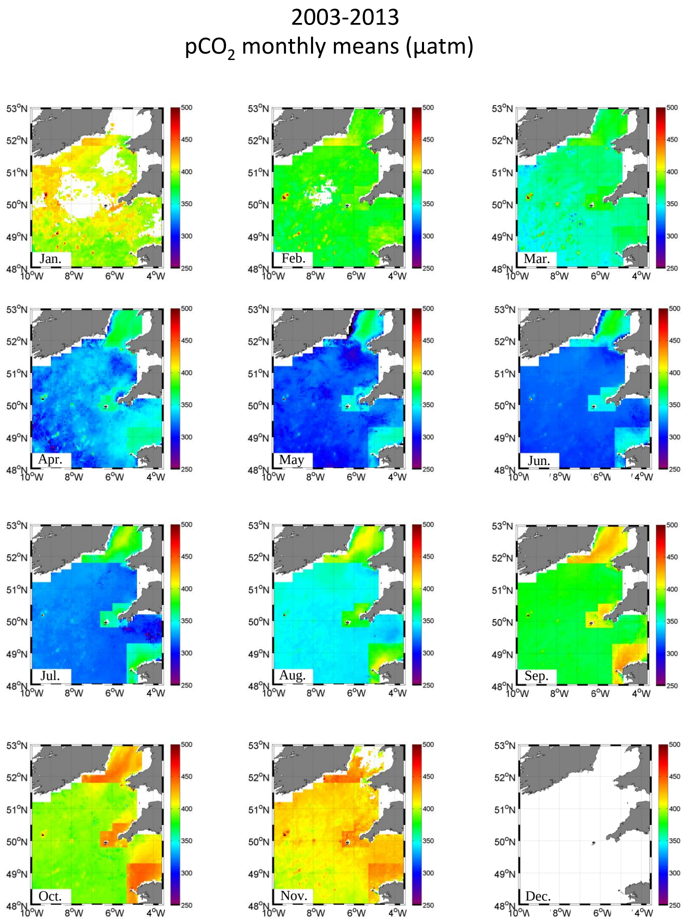

Figure 11. Monthly $pCO_{2,MLR}$ (µatm) computed from the algorithms developed in seasonally stratified and in permanently well-mixed systems averaged from 2003 to 2013 from January (top left corner) to December (bottom right corner).

BGD
12, 5641–5695, 2015

Title Page
Abstract | Introduction
Conclusions | References
Tables | Figures
◀| |▶
◀ ▶
Back | Close
Full Screen / Esc
Printer-friendly Version
Interactive Discussion

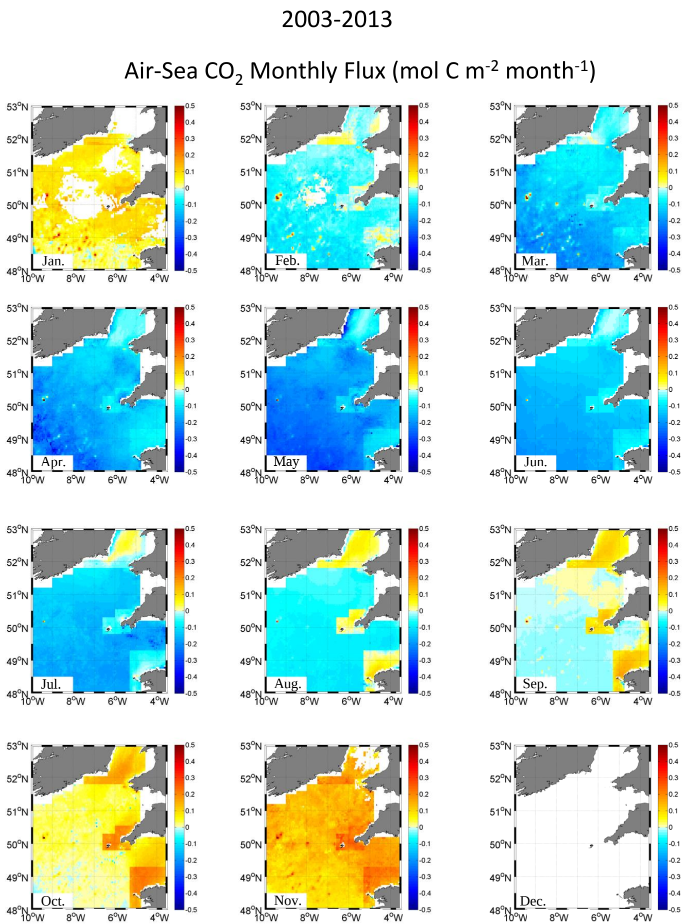

Figure 12. Monthly air–sea CO_2 fluxes (mol C m^{-2} month^{-1}) computed from $p\mathrm{CO}_{2,\mathrm{MLR}}$ and using Nightingale et al. (2000) K-wind relationship averaged from 2003 to 2013 from January (top left corner) to December (bottom right corner). Negative values indicate CO_2 sink.

BGD
12, 5641–5695, 2015

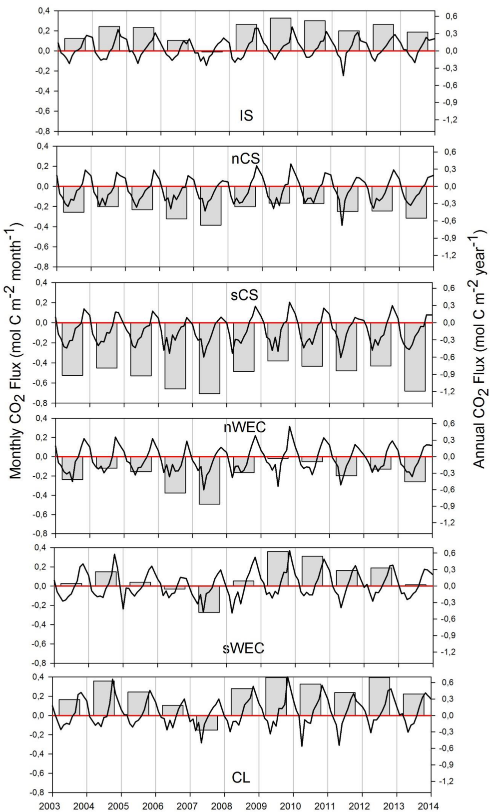

Figure 13. Monthly air–sea CO_2 fluxes (black lines, left hand side *Y* axis, mol C m^{-2} month^{-1}) computed from $pCO_{2,MLR}$ and using Nightingale et al. (2000) *K*-wind relationship in IS **(a)**, nCS **(b)**, sCS **(c)**, nWEC **(d)**, sWEC **(e)** and CL **(f)** provinces from 2003 to 2013. Negative values indicate CO_2 sink. Integrated annual CO_2 fluxes (vertical grey bars, right hand side *y* axis, mol C m^{-2} year^{-1}).

BGD
12, 5641–5695, 2015

Dynamics of air–sea CO_2 fluxes in the N-W European Shelf

P. Marrec et al.